Tectonic and sedimentary history of the Neoproterozoic metavolcanic- volcaniclastic rocks of the El-Dabbah Group, Central Eastern Desert, Egypt

Kiyokawa, Shoichi
Department of Earth and Planetary Science, Kyushu University

Suzuki, Taishi
Department of Earth and Planetary Science, Kyushu University

Horie, Kenji
National Institute of Polar Research

Takehara, Mami
National Institute of Polar Research

他

出版情報：Journal of African Earth Sciences. 165, pp.103807-, 2020-05. Elsevier
バージョン：
権利関係：

Tectonic and sedimentary history of the Neoproterozoic metavolcanic–volcaniclastic rocks of the El-Dabbah Group, Central Eastern Desert, Egypt

Shoichi Kiyokawa[a,b,c], Taishi Suzuki[a], Kenji Horie[d], Mami Takehara[d], Hanna El-Dokouny[e], Al-Dekouny Maher Dawoud[e], Mohamed Mahmoud El-Hasan[e]

[a] Department of Earth and Planetary Science, Kyushu University, 744 Motooka Nishiku, Fukuoka 819-0395, Japan

[b] Department of Geology, University of Johannesburg, PO Box 524, Auckland Park, Johannesburg 2006, South Africa

[c] Center for advanced Marine core research, Kochi University, B200 Monobe, Nankoku, Kochi, 783-8502, Japan

[d] National Institute of Polar Research, 10-3 Midori-cho, Tachikawa-shi, Tokyo 190-8518, Japan

[e] Department of Geology, Faculty of Science, Menoufiya University, Gamal Abd El Nasr st. Shebin El-Kom, Menoufiya, Egypt

Corresponding author

Shoichi Kiyokawa: kiyokawa@geo.kyushu-u.ac.jp

Tel. 092-802-4254

Email addresses

Taishi Suzuki: t14851295@gmail.com

Kenji Horie: horie.kenji@nipr.ac.jp

Mami Takehara: takehara.mami@nipr.ac.jp

Al-Dekouny Maher Dawoud: dawoud_99@yahoo.com

Mohamed Mahmoud El-Hasan: abouelhassanmohamed@gmail.com

Hanna Abd-Elmonem: hanaaabdelnaby4@gmail.com

Abstract

The El-Dabbah Group is a > 7500m-thick sequence of metavolcanic rocks, volcaniclastics, and banded iron-formation located within the Nubian Shield, Central Eastern Desert, Egypt. The sequence preserves lower greenschist-facies island arc rocks. We used detailed mapping to reconstruct the stratigraphic and tectonic history of the El-Dabbah Group and the surrounding sedimentary basins. The El-Dabbah Group was identified as deposition at central rift zone of an oceanic island arc and was overlies by the subaerial sedimentary rocks (the Atshan Formation and the Hammamat Group). Four faulting were distinguished within the El-Dabbah area: (1) top-to-the-S low-angle thrusting; (2) NNE side down normal faulting; (3) sinistral displacement on north–south faults; and (4) WNE trend N-side-down normal faulting with the Hammamat Group. We obtained the crystallization ages of a granite (638.1 ± 2.9 Ma) and a quartz porphyry (659.6 ± 3.0 Ma). The detrital zircon age of the Hammamat Group show peaks at 650, 680, and 790 Ma. These evidences suggest, three sedimentation-deformation stages were identified in this area. Stage 1 involved sedimentation of island-arc-derived volcaniclastic rocks at 770-700 Ma and to thrust related accretion at 700–680 Ma. Stage 2 involved collisional and transtensional deformation related to formation of the subaerial basin that contains the Atshan Formation at 670-640 Ma, the normal fault, the strike-slip fault and granite intrusion during 660–620 Ma. Stage 3 involved orogenic collapse, regional strike-slip-related sedimentation and deformation of the Hammamat Group at 610–570 Ma. We show that the El-Dabbah Group records a history of oceanic island arc accretion, collision, and collapse within the northern East African Orogeny during 770-570 Ma in Neoproterozoic.

Keywords: Neoproterozoic, El-Dabbah Group, Hammamat Group, oceanic island arc, volcaniclastic sequence, accretion, transtension,

Highlights

- Three stages of sedimentation and deformation were identified in the El-Dabbah area
- A 7500 m-thick sequence of metavolcanic and volcaniclastic rocks formed in an oceanic island arc setting
- Three stages of sedimentation (Sed 1-Sed 2) and deformation (D_1–D_3) occurred in the El-Dabbah area
- Granite and quartz porphyry intrusions crystallized prior to D_2, at 660–640 Ma.

1. Introduction

The Eastern Desert of Egypt is an escaped tectonic block within the northern part of the East African Orogeny which was older part of the Pan-African Orogeny (Fritz et al., 2013), the escape of the block occurred during collision between East and West Gondwana (e.g., El-Gaby et al., 1984, Stern 1994). The Egyptioan Eastern Desert contains well-preserved accreted sections of island arc rocks, granitic rocks, and exhumed metamorphic rocks, and has been subdivided into three terranes: Northern Eastern Desert

(NED), Central Eastern Desert (CED), and Southern Eastern Desert (SED), based on rock types and ages (Stern and Hedge, 1985, Fowler and Hamimi, 2020).

Low-grade metamorphic assemblages are well preserved within the basement rocks of the CED, which include ophiolitic mélange, metavolcanic island arc rocks, subaerial sedimentary rocks, and granites that are older and younger than the accretion event (e.g., Egyptian Geological Survey, 1981; El-Shazly and Khalil, 2016). The area records lower pressures than the NED and the SED, so the pre-metamorphic relationships amongst the units are well preserved.

The basement rocks of the CED can be divided into three major sections; (1) a gneiss complex; (2) island arc metavolcanic rocks and sediments; and (3) late- to post-orogenic Hammamat Group sediments (El-Gaby et al., 1984). The gneiss complex has been interpreted as an extensional core complex dome or early thrust-stacking with later folding dome models (e.g., Fritz et al., 1996, 2002; Fowler et al., 2007; Hamimi et al., 2012). Thick sequences of island arc metavolcanic rocks and sediments, and a tectonic mélange that contains ophiolitic rocks, were accreted at the early stage (Stern et al., 2004; Fritz et al., 2013). Early stage accretional deformations are still difficult to distinguish.

Most of the island arc metavolcanic rocks and sediments, other than those of the Hammamat Group, experienced greenschist-facies metamorphism with brittle deformation and minor brittle–ductile deformation (e.g., El-Shazly and Khalil, 2016). These low-grade island arc metavolcanic rocks and sediments sequence might be preserved early stage deformations.

A sequence of low-grade metavolcanic and volcaniclastic rocks are exposed in the Wadi El-Dabbah area of the CED (e.g., Maurice, 2006; Ali et al., 2009). These rocks are located between the well-studied El-Sibai complex area (e.g., Fowler et al., 2007) and the Kareim basin (240 km^2) containing the Hammamat Group within the CED. Subaerial sediments of the Hammamat Group unconformably overlie the arc metavolcanics at southern margin of the Kareim basin. Therefore, the metavolcanic–volcaniclastic sequence was emplaced prior to sedimentation of the Hammamat Group (Wilde and Youssef, 2002; Abd El-Wahed et al., 2010) and might record the tectonic and sedimentary history of this area, which includes formation of the island arc, tectonic mélange, thrust nappes, post-accretion deformation, and granite intrusion (e.g., Ali et al., 2009; Khalil et al., 2015).

However, detailed geological mapping and stratigraphic studies have not been conducted in this area. We performed detailed mapping, structural investigations, stratigraphic reconstructions, and geochronology analyses. We did not observe a mélange similar to those recorded accreted tectonic mélange within Japanese accretionary complexes (e.g., Kiyokawa, 1992). The metavolcanic–volcaniclastic sequence of the El-Dabbah area contains well-preserved volcano-sedimentary structures (such as, pillow lava, accretionary lapilli, graded volcanic tuff, parallel laminated tuff and iron sequence) that were used to reconstruct a continuous stratigraphy, and on this basis we inferred that the sediments were formed in an island arc setting. New detrital zircon U–Pb ages of the Hammamat Group sandstone, and igneous zircons from two intrusions constrain the timing of sedimentation and fault movement.

Finally, we compare the tectonic histories of the sedimentary basin, gneiss complex, and the metavolcanic–volcaniclastic sequence.

2. Regional tectonic history of the Central Eastern Desert

2.1. Tectonic framework of the Eastern Desert

The Eastern Desert of Egypt is part of the Arabian–Nubian Shield. It was previously part of the Arabian Plate, and part of the Rodinia supercontinent prior to its breakup at ~900–850 Ma. This breakup event is recorded by ~870 Ma Neoproterozoic juvenile volcanic rocks, which include an island arc sequence (Stern, 1994) that was accreted during collisional events related to the East African Orogeny which was older part of the Pan-African Orogeny and closure of the Mozambique Ocean (Stern 1994; Cawood, 2005; Fritz et al., 2013; Fig. 1). The tectonic history of the Arabian–Nubian Shield comprises seven stages: (1) breakup of Rodinia (900–850 Ma); (2) seafloor spreading to form oceanic lithosphere (870–750 Ma); (3) subduction and formation of island arc volcano-sedimentary sequences (760–720 Ma); (4) accretion and collision of the island arc sequence; (5) intrusion of older granites (760–610 Ma); (6) exhumation and orogenic collapse (600–570 Ma); and (7) intrusion of alkalic, post-orogenic younger granites (570–474 Ma) (Stein and Goldstein, 1996; Johnson and Woldehaimanot, 2003; Meert, 2003; Stern, 2003; Fowler and Osman, 2013; Fritz et al., 2013; El-Shazly and Khalil, 2016; Hamimi et al., 2020; Fowler and Hamimi, 2020).

Most of the Arabian–Nubian crust was generated by circum-Mozambique Ocean intra-oceanic arc systems (Tadesse et al., 1999; Woldehaimanot, 2000). When the Mozambique Ocean closed, these juvenile island arc and oceanic plateau terranes were amalgamated by collision and accretion to form larger tracts of juvenile crust that probably accreted onto pre-existing juvenile continental crust (Stein and Goldstein, 1996; Stern, 2003). Continued collision produced arc–arc sutures and composite terranes that formed the juvenile Arabian–Nubian Shield (Johnson and Woldehaimanot, 2003; Fowler and Hamimi, 2020).

Convergence among the fragments of East and West Gondwana, and the resulting East African Orogeny, continued with increasingly intense deformation during the Ediacaran (630–550 Ma; Veevers, 2003). The northern East African Orogeny formed strike-slip shear zones and tectonic collapse structures in Egypt, Sudan, and northern Arabia, and generated and exhumed high-grade gneisses and a granulite complex (Abdelsalam and Stern, 1996; Fritz et al., 1996, 2002, 2013; Neumayr et al., 1996, 1998; Abd El-Wahed, 2007, 2008).

In the Eastern Desert, the NED contains serpentinites, post-orogenic younger granites (<570 Ma), the Dokhan volcanic arc rocks (602–593 Ma; Wilde and Youssef, 2000), and faults and joint sets (Hamimi et al., 2019). The CED is composed mainly of a 750–700 Ma rocks that comprises disrupted ophiolitic mélange, a relatively low-grade volcanic–volcaniclastic sequence with iron formations, shallow-water basin sediments, and high-grade metamorphic complexes. (Hamimi et al., 2019). The SED is composed

mainly of the older granites (>630 Ma), a high-grade metamorphic sedimentary sequence, and voluminous gneiss and migmatite. Deformation within the SED is dominated by folding related to thrusting, and is overprinted by regional-scale transpression (Hamimi et al., 2019). Subduction is thought to have been towards the N–NNE during the early stages of collision (e.g., Abd El-Naby and Frisch, 2002; Abdeen and Abdelghaffar, 2011; Fowler and Hamimi, 2020), based on the presence of ophiolite fragments within the suture.

2.2. Tectonic framework of the Central Eastern Desert

Thrusting related to collision, and subsequent intense strike-slip deformation affected the accreted island arc metavolcanic sequence of the CED (Loizenbauer et al., 2001; Shalaby et al., 2005; Abd El-Rahman et al., 2009; El-Shazly and Khahlil, 2016; Abd El Wahed et al., 2019; Hamimi and Abd El-Wahed, 2020). High-grade metamorphic rocks of the El-Sibai and Meatiq complexes were exhumed by 12–15 km during crustal extension at ~620–580 Ma to form gneiss dome (core) complexes (Loizenbauer et al., 2001; Hamimi et al., 2019). The complicated metavolcanic sequence was emplaced above crustal rocks (Fritz and Messner, 1999) and has been interpreted as an ophiolitic mélange (e.g., Stern et al., 2004; Ali et al., 2009; Khalil et al., 2015), or collision–accretion nappe sheets related to the Pan-African nappe complex (Bregar et al., 2002).

Intense strike-slip deformation on the Najd fault system, which extends into Saudi Arabia, overprinted earlier deformation (e.g., Johnson, 2014). The strike-slip fault system exhumed high-grade rocks to form core complexes that contain mid-crustal, amphibolite–granulite-facies rocks that record extensional deformation (Fritz et al., 1996, Loizenbauer et al., 2001). Fowler et al. (2007) suggested that the El-Sibai gneiss complex consists of folded nappe sheets rather than an exhumed mid-crustal core complex. Rocks within the gneiss complex yield ages of 685–680 Ma, which are interpreted as the timing of arc-related thrusting on an early low-angle thrust system that is preserved within the gneiss complex (Fowler et al., 2007; Augland et al., 2012). The causes of the deep crustal deformation, early accretion, and collision are debated (e.g., El-Bialy, 2019).

The El-Dabbah area also contains a well-preserved strike-slip shear zone that includes crustal-scale wrench faults. Northwest–southeast-trending strike-slip transtensional deformation affected the metamorphic gneiss complex and the Hammamat Group (Fritz et al., 1996; Fritz and Messner, 1999; Loizenbauer et al., 2001; Abd El-Wahed, 2010). This younger deformation of the crustal basement rocks and covering sediments was related to post-deformation orogenic collapse on the Najd fault system in the CED (e.g., Fritz et al., 2013).

2.3. Distribution of the Hammamat Group

The Hammamat Group was formed on the subareal sedimentary basins, which was 25 exposed area_ preserving mainly in the CED (Fowler and Osman, 2013). These are inferred to have formed in a range of tectonic settings (e.g., continental margin, transpressional, extensional rifts; Fowler and Osman, 2013). The Kareim Basin is one of the largest sedimentary basins that preserves the Hammamat Group within

the CED. Rocks of the Kareim Basin are well exposed in a synform that consists of shallowly N- and S-dipping strata in the northwest Wadi El-Dabbah area. The basin contains a coarsening-upward mega-sequence of ~7500 m of continuous lacustrine to coarse alluvial facies sediments (Fritz and Messner, 1999). The basin is interpreted as a tectonically controlled pull-apart basin that formed in response to strike-slip deformation on the Najd Fault system (Stern, 1985). Basin sedimentation, which constrains the timing of onset of strike-slip deformation, is thought to have been linked to movement on the NW–SE-trending Najd fault system, which caused regional deformation (e.g., the East Arabian Orogeny; Fowler and Osman, 2001; Shalaby et al., 2005; Fritz et al., 2013). However, detailed structural studies indicate that early sedimentation within the Kareim basin occurred within a subsiding basin adjacent to the exhumed core complex and associated igneous rocks (Fritz et al., 1996; Fritz and Messner, 1999). The subsiding deformation to make the Kareim basin was related to oblique convergence and transtensional deformation (Fritz et al., 1996; Fritz and Messner, 1999). However, strike-slip deformation only occurred toward the end of sediment deposition within the Kareim basin, based on observed fault offsets and the distribution of coarse grain sediments in the upper part of the sequence (Fritz and Messner, 1999).

The detrital zircon U–Pb age spectra of the NED Hammamat Group samples from Gebel Umm Tawat are characterized by primary peaks at 680 and 640 Ma and a minor peak at 585 Ma (Bezenjani et al., 2014). The ages of the primary peaks are similar to the ages of older granites related to island arc formation, and the age of the minor peak is similar to the age of the Dokhan volcanic rocks of the NED (602–593 Ma; Wilde and Youssef, 2000, 2002). In addition, sandstones of the Igla Basin near Masa Alam in the SED preserve young zircon ages (628 Ma) (Bezenjani et al., 2014). The Hammamat Group was deposited at 620–580 Ma over a wide area that included multiple basins (Shalaby et al., 2006). The Hammamat Group sediments constrain the timing of exhumation of the sediment source area and the timing of basin formation.

3. Structural interpretation of the Wadi El-Dabbah area

To identify the stratigraphy in this area, reconstructed structural frameworks should be prepared from detail mapping. Based on detailed geological maps and structural observations, we identified four geological units in the Wadi El-Dabbah area, (Figs. 2, 3): (1) a metavolcanic–volcaniclastic sequence, assigned to the El-Dabbah Group that consists of island-arc-related metavolcanic and volcaniclastic rocks (Fritz and Messner, 1999); (2) a metamorphosed subaerial sedimentary basin defined as the Atshan Formation; (3) a less-deformed terrigenous sedimentary basin (the southern Kareim basin) that is interpreted as the Hammamat Group sediments (Fritz and Messner, 1999; Wilde and Youssef, 2002); and (4) weakly deformed granite and porphyry intrusions.

The metavolcanic–volcaniclastic rocks of the El-Dabbah Group experienced lower greenschist-facies metamorphism under pressure–temperature conditions of 373°C ± 61°C and 1.1–2.2 kbar (El-Shazly and Khalil, 2016). The rocks can be subdivided into four fault-bounded domains (Fig. 3): the northeast (NE),

southeast (SW), northwest (NW), and southwest (SW) domains. The El-Dabbah Fault is located within the N–S-trending Wadi El-Dabbah and the E–W-trending and N-dipping normal faults are subdivided into four domains. The eastern boundary of the metavolcanic–volcaniclastic sequence is a NW–SE-trending fault and the western boundary is a N–S-trending fault that separates the sequence from the Atshan Formation. The northern boundary is an unconformable contact with the overlying Hammamat Group and the southern boundary is an intrusive contact with granite (Fig. 3).

3.1. Faults

Four generations of faulting were identified in the Wadi El-Dabbah area, based on mapping and field observations (Fig. 3). The first generation, F_1, affects rocks of the El-Dabbah Group and produced thrust faults that are sub-parallel to layering and dip shallowly to the north (Fig. 4A). Asymmetric tight to isoclinal folds with sub-horizontal NW–SE- axes are preserved along the faults (Fig. 4B). Asymmetric folds shape record top-to-the-south slip. The footwalls volcaniclastic rocks, sometimes contain sub-vertical fault plane open-crack quartz veins (such as, tension gash, comb fractures), however, slikenline or stretching lineations on the fault planes are not well preserved.

The second generation of faulting, F_2, produced normal faults that dip to the NNE and form the boundaries between the NE domain and the SE domain and the NW domain and the SW domain. Some of the normal faults occur within the metavolcanic–volcaniclastic sequence (Fig. 4C, D). The fault planes are well preserved with slikenline or stretching lineations with fibers steps which features record northside down movement. The volcaniclastic beds are observed in drag-folds related to the normal faults. Moderately to intensely developed stretching fabrics occur in the footwall sequence.

Boundary between the El-Dabbah and Atshan formations (Fig. 4E) is also identified as a NW-side-down F_2 normal fault. This fault cuts the stratigraphically lower parts of the El-Dabbah Group metavolcanic–volcaniclastic sequence and the conglomerate–sandstone sequence of the Atshan Formation. A quartz porphyry that intrudes the Atshan Formation is truncated by this fault (Fig. 3).

The third generation of faulting, F_3, is represented by the El-Dabbah Fault, a N–S-striking sinistral strike-slip fault (Fig. 3). The total displacement on this fault is ~800 m, based on offsets between domain boundaries and F_2 faults of the east and west domains. It is also identified as a displacement of iron-formation marker beds with mappable asymmetric folding at Wadi El-Dabbah (Fig. 4F), and displacement of a massive hornblende–biotite granite (Fig. 4G). The north-south striking El-Dabbah Fault is not observed at the northern end of the wadi outcrops in wadi branch RW 00 (Fig. 3). This indicated the F_2 fault between the El-Dabbah and Atshan formations and at the RW 00 branch may be cut of the El-Dabbah Fault. The F_2 between the El-Dabbah and Atshan formations also preserves shallow dipping sheared lineation and may be overlapped by sinistral deformation. In this way, the F_2 between the El-Dabbah and Atshan formations may be reactivated by F_3 faulting strike-slip deformation.

The fourth generation of faulting, F_4, is represented by small normal faults in the NW domain that record 10–20 m of displacement. The unconformity between the volcaniclastic rocks of the El-Dabbah Group and the red sandstone beds of the Hammamat Group is truncated by a normal fault of this generation. Movement on this fault has displaced the unconformity by tens of meters.

3.2. Structure of the metavolcanic–volcaniclastic sequence

3.2.1. Northeast domain

The NE domain of the metavolcanic–volcaniclastic sequence is bounded by a NW–SE-trending $F_{2\,(3)}$ strike-slip fault to the east of the Atshan Formation, and the El-Dabbah Fault to the west. The total thickness of the El-Dabbah Group in the NE domain is 600–1000 m. The strata in this domain are relatively undeformed, dip at 20°–40°, and form an open fold that plunges shallowly to the east (Fig. 3). The lowest unit within the southern and southeastern parts of the NE domain contains thick metavolcanic rocks that consist of stratified lavas and pillow lavas (Fig. 5A). A thin layer of iron formation is preserved within the volcaniclastic rocks. The middle unit occurs in the central parts of this domain and contains massive pillow lavas and massive yellow volcaniclastic sediments. The uppermost unit occurs in the northern part of this domain and consists of a bedded volcano–sedimentary sequence.

3.2.2. Southeast domain

The SE domain is bounded by the El-Dabbah Fault to the west, a WNW–ESE-trending and north-side-down F_2 normal fault to the north (Fig. 4A), and an intrusive contact with massive granite to the south. Contact metamorphic evidences of the granite intrusion are not well preserved in this area. The total thickness of the El-Dabbah Group within this domain is ~5 km. This domain is divided into a massive volcanic rock unit (>4-km-thick) and a volcaniclastic sedimentary rock unit (600–1000 m thick).

The massive volcanic rock unit consists of massive coarse basalt and foliated coarse basalt (Fig. 3). The strata in this domain commonly dip at 40°–70° towards the N and NE. This unit contain massive coarse basalts, fine dolerite and or microgabbro (Fig. 5B). Layers within the massive volcanic rocks are commonly >40 m thick. The rocks contain brittle joints, but columnar jointing was not observed. Individual lava flows were not recognized, and we interpret this unit as a crystallized subvolcanic body or a magma chamber that formed below the volcanic rocks. This unit is the stratigraphically lowest unit of the El-Dabbah Group.

The volcaniclastic sedimentary rock unit is 600–1000 m thick and consists of a sequence of well-preserved bedded and laminated rocks that include a greenish shale that was interpreted as a volcanic tuff, iron formations (Fig. 4A, F), thick layers of metavolcanic rocks, and pillow lavas (Fig. 5C). The stratigraphy is well constrained by continuous exposure from the massive volcanic rock unit to the volcaniclastic sediment unit. The well-bedded volcaniclastic rocks and the banded iron formation (BIF) are well exposed on the eastern wadi bluff between branches RE 03 and RE 08 of Wadi El-Dabbah (Fig. 4F). The volcaniclastic sedimentary unit is more intensely foliated in this domain than in the other domains.

3.2.3. Northwest domain

The NW domain is transected by a well-preserved N-dipping F_2 normal fault and bounded to the east by the El-Dabbah Fault. The northern boundary is an unconformity between the NW domain and conglomerate and sandstone of the Hammamat Group. North-dipping normal faults occur in this domain (Fig. 4C, D). A well-stratified volcaniclastic sedimentary sequence well preserved and total thickness of is 700–1200 m. Massive greenish volcanic tuffs and pillow basalts are well preserved within this sequence. Thin iron formations, 5–10 cm thick, are preserved within thick beds of massive volcanic tuff bed. Volcaniclastic beds oriented shallowly dipping and NW- shallow plunge open folds structure (Fig. 2). Red sandstones of the Hammamat Group lie unconformably above the metavolcanic unit at topographic highs (Fig. 5D). The NE-dipping, small-scale normal faults (F_4) shows offsets of unconformity plane up to several meters.

3.2.4. Southwest domain

The SW domain is bounded to the north by a N-dipping fault (F_2), to the east by the El-Dabbah Fault (F_3), and to the west by a N–S-trending F_3 fault within the Atshan Formation, which consists of muddy sandstone and conglomerate. The southern boundary of this domain is an intrusive contact against an undeformed hornblende–biotite granite (Fig. 4G). Contact metamorphic evidences of the granite intrusion are not well preserved in this area. The strata in this domain commonly dip to the N at 40°–60°, and stratigraphic repetition caused by faulting was observed within the continuous exposure.

The total estimated thickness of the El Dabbah Group in this domain is ~4200 m, excluding duplication by thrust faulting. Three stratigraphic units occur in this domain: massive volcanic rocks, BIF rich volcaniclastic rocks, and tuff rich volcaniclastic rocks. The massive volcanic rocks unit is ~800 m thick and comprises layers of metavolcanic rocks, microgabbros, and small amounts of volcaniclastic rocks that include thin iron-rich beds. Lowest boundary is intruded contact with granite.

The BIF rich volcaniclastic rocks unit consists of pillow lavas, bedded tuffs (Fig. 5E), black shales, iron-rich beds within the shales and BIF (Fig. 5F). Accretionary lapilli tuffs occur within the volcaniclastic layers (Fig. 5E). Isoclinal fold is preserved within the BIF (Fig. 4B), which also records thrusting sub-parallel to layering. Duplication of the stratigraphy was not observed within the thrust faults, and the unit is about 2400 m thick, based on the minimum thickness calculated from exposed stratigraphic sequences in this domain.

The tuff rich volcaniclastic unit is >1000 m thick and comprises massive basaltic lavas, pillow lavas (Fig. 5H), and thick fine bedded tuffs with minor iron-rich beds. Upper portion was divided by north dipping normal fault.

4. Stratigraphy of the Wadi El-Dabbah area

We undertook a detailed stratigraphic reconstruction of the El-Dabbah Group, Atshan Formation, and Hammamat Group in the Wadi El-Dabbah area (Figs. 3, 6).

4.1. El-Dabbah Group

The El-Dabbah Group is defined for the first time in the present study. It is a metavolcanic–volcaniclastic sequence that has been interpreted as a Pan-African nappe sequence or an accreted section of island arc material (e.g., Ali, 2009; El-Shazly and Khalil, 2016). We integrated stratigraphic data from the NE, SE, NW, and SW domains to produce the stratigraphic framework. Distinctive beds (e.g., BIF, thick basaltic pillow lava) were identified and used to correlate the strata in each domain to define the stratigraphy. The formation thicknesses are approximate and based on current exposures.

The El-Dabbah (ED) Group is divided into the Lower ED, Middle ED, and Upper ED formations (Fig. 6). The total thickness of the group is ~7500 m, stratigraphic overlap portion in each domain is shown in Fig. 6.

The massive volcanic rock unit represents the Lower ED Formation in the SE and SW domains. The total thickness is ~4000 m. This unit consists of coarse-grained massive volcanics and microgabbro interbedded with thin layers of volcaniclastic rocks and minor fine-grained dolerite. The lower boundary of this unit is poorly constrained because the lowest parts of the stratigraphy are intruded by the hornblende–biotite granite (Fig. 4G). The upper parts of the Lower ED Formation consist of thin layers of volcaniclastic rocks and iron-rich and jasper-bearing beds. The well-preserved pillow basalts and thin graded tuff beds indicate that the unit youngs towards the north.

The Middle ED Formation is represented by the ~2500-m-thick, from volcaniclastic sedimentary rock unit in the SE domain and the volcaniclastic–BIF unit of the SW domain. It contains numerous massive basaltic lavas, pillow lavas, and a metavolcanic–volcaniclastic sequence that is interbedded with fine-grained tuff beds, iron-rich beds, and BIF. This formation is subdivided into the BIF Member and the Volcaniclastic Member (Fig. 6). The BIF Member consists of basal massive lava flows, pillow lavas, and thick-bedded volcaniclastic rocks, with a number of fine-grained sedimentary sequences that include finely laminated volcanic rocks, black shales, iron-rich beds, and BIF. The volcaniclastic rocks and basaltic pillow lavas form beds that are a few meters thick (Fig. 5C, H) and occur within tuffs and BIF. The BIF includes thin jasper layers, typically 2–4 m thick, that crop out on both banks of Wadi El-Dabbah (Figs. 4F, 5G). A fine-grained mudstone section with graded bedding is preserved within the thin volcaniclastic tuff and black shales (Fig. 5F). The Volcaniclastic Member contains a thick (10–40 m) succession of volcaniclastic rocks, basaltic pillow lavas and some BIF. The well-preserved basaltic pillow lavas show flow and sag features, and horizontal lava tubes occur on one side of the pillow lavas. These structures record younging to the north. The volcaniclastic sequence contains accretionary lapilli beds that are one to three meters thick with well round 0.5 to 1 cm diameter grains with few mm thick fine material coated texture (Fig. 5E). Some BIF (less than 1m) preserved within fine volcaniclastic sequence.

The Middle ED Formation within the SW domain is at least three times thicker than the comparable volcaniclastic sedimentary unit of the SE domain (600–1000 m). This difference in thickness might be related to late-stage normal faulting (see below).

The Upper ED Formation is represented by the volcanic lava–volcaniclastic unit of the SW domain and the metavolcanic–volcaniclastic sequence of the NE and NW domains. The total thickness is at least 1000 m, and the formation comprises volcaniclastic sediments, minor basaltic pillow lavas, and extensively reworked cross-stratified volcaniclastic rocks. Accretionary lapilli tuffs are partly preserved within greenish volcaniclastic sediments. Thin iron-rich beds and black shales are intercalated with greenish volcaniclastic rocks and basaltic pillow lavas (Fig. 5C). The upper boundary of the formation is defined by the unconformity below the Hammamat Group (Fig. 5D). Fault contacts with the Atshan Formation are also observed.

4.2. Atshan Formation

The Atshan Formation occurs to the east and west of the El-Dabbah Group, and in the Wadi Atshan area. This formation is bounded by faults and is weakly to intensely foliated and deformed.

To the west of the SW domain of the El-Dabbah Group, the Atshan Formation comprises a muddy matrix-supported conglomerate with cross-bedded and laminated sandstone (Fig. 7A). The conglomerate comprises angular–subangular clasts of greenish and black volcanic rocks in a mud-rich matrix (Fig. 7B). Vesicular volcaniclastic breccias occur within the conglomerate. The conglomerate and sandstone unconformably overlie steeply dipping metavolcanic rocks of the El-Dabbah Group and are cut by a basaltic dike with an irregular contact (Fig. 7A). The Atshan Formation is unconformably overlain by well-sorted sandstones and conglomerates of the Hammamat Group on flat hilltops.

Well-preserved bedded sandstones containing mud drapes and well-sorted laminated sandstones with layers of rounded pebbles are exposed in cliff sections within Wadi Atshan, 2 km north of Wadi El-Dabbah (Fig. 7C–E). This sequence is intensely folded in places and cut by normal faults (Fig. 7C). The sandstone sequence is unconformably overlain in places (e.g., the middle of the cliff section) by muddy conglomerates of the basal Hammamat Group (Fig. 7C, E).

Northeast of the NE domain of the El-Dabbah Group, the Atshan Formation comprises well-bedded sandstone containing mud drapes, rhythmically laminated sandstones and mudstones interpreted as varves, beds of well-rounded pebbles, and debris flow sediments with a muddy matrix (Fig. 7F, G). This portion identified as lacustrine condition. The total thickness of the Atshan Formation is ~1000 m, and the rocks are folded and dip steeply (Fig. 7F). The Atshan Formation is intruded by a quartz porphyry that is strongly foliated cut by strike-slip related normal fault (F_2 and F_3) that also cuts the NW and the SW domains of the El-Dabbah Group. The intense folding, shearing, and poor exposure prevented a detailed evaluation of the stratigraphy of the Atshan Formation.

4.3. Hammamat Group

The Hammamat Group occurs on the southeastern margin of the Kareim basin in the Wadi El-Dabbah area, where it is represented by a red fluvial–lacustrine sedimentary sequence (Fig. 7H) that unconformably overlies the El-Dabbah and Atshan formations. A well-preserved unconformity between the Hammamat and El-Dabbah groups occurs within hilltops of the NW domain of the El-Dabbah Group.

The basal parts of the Hammamat Group are dominated by coarse sandstones with quartz pebbles that occur within a few meters of the base. Thick red–purple shales and sandstones occur above the basal sequence. The sandstone sequence is tilted northward by small-scale normal faults (F_4) in the NW domain. The red and purple shales show a strongly developed fold-related cleavage.

5. Uranium–lead zircon geochronology

Zircon U–Pb dating of the Hammamat Group basal sandstone (Fig. 5D), a quartz porphyry intrusion, and the hornblende–biotite granite (Fig. 4G) was used to constrain the relative ages of sedimentation, fault movement, and magmatism in the Wadi El-Dabbah area.

The Hammamat Group was deposited after the Atshan and El-Dabbah groups were deformed. The quartz porphyry intruded the Atshan Formation along a strike-slip normal fault (F_2 and F_3) that cuts the El-Dabbah Group, so the age of the porphyry constrains timing of the Atshan Formation sedimentation and strike-slip normal fault movement (Fig. 4E). The hornblende–biotite granite (Fig. 4G) intruded the southern margin of the El-Dabbah Group and constrains the age of granitic magmatism and the El-Dabbah Fault (F_3).

5.1. Analytical methods

The samples were cleaned with deionized water in an ultrasonic bath for >5 min, and then disaggregated using a high-voltage pulse–power fragmentation device (SELFRAG Lab) at the National Institute of Polar Research (NIPR), Japan, which eliminates contamination during crushing and pulverizing. The zircon grains were concentrated using conventional mineral separation techniques, including heavy liquid separation with methylene iodide and magnetic separation. The zircon grains were handpicked and we ensured that the selected grains were representative of the zircon population. Approximately 200 zircon grains were mounted within an epoxy resin disc along with the reference material. After curing, the disc was polished to expose cross-sections through the grain centers and coated with carbon for observation. Back-scattered electron (BSE) and cathodoluminescence (CL) images were obtained using a JEOL JSM-5900LV scanning electron microscope (SEM) with a Gatan mini CL detector at the NIPR, and used to characterize the internal zoning and identify suitable analysis sites within each zircon grain. Subsurface mineral inclusions and cracks were identified using an optical microscope under transmitted light. Prior to analysis by sensitive high-resolution ion microprobe (SHRIMP-II), the surface of the grain mount was washed with dilute HCl and ultrapure water, and coated with gold. After SHRIMP analysis, the grain mounts were coated with carbon and true-color CL images were obtained using a Gatan ChromaCL2 with a field-emission SEM (JEOL JSM-7100F) at NIPR, using an electron beam current of ~2.7 nA and acceleration voltage of 3 kV.

The U–Pb dating was undertaken using a SHRIMP-II ion microprobe at NIPR. An O_2^- primary ion beam of 3.2–5.2 nA was used to sputter analytical spots of ~25 μm diameter on each polished zircon grain. The procedures for Pb and U isotope analyses follow those of Horie et al. (2013) and references

425 therein. In this study, TEMORA2 ($^{206}Pb/^{238}U$ age = 416.78 ± 0.33 Ma; Black et al., 2004) and SL13 (U =
426 238 ppm; Claoué-Long et al., 1995) were used as reference zircons to calibrate the $^{206}Pb/^{238}U$ ratios and U
427 concentrations, respectively. Zircon standards FC1 (1099 Ma; Paces and Miller, 1993) and OG1
428 ($^{207}Pb/^{206}Pb$ age = 3465 Ma; Stern et al., 2009) were also analyzed periodically with TEMORA2 to
429 monitor the U/Pb signal and instrumental mass fractionation. The U–Pb data were reduced following the
430 procedures of Williams (1998), using the SQUID2 Microsoft Excel macro developed by Ludwig (2009).
431 Common Pb was corrected using measured ^{204}Pb and the model of common Pb of Stacey and Kramers
432 (1975). The ages were calculated after correction for common Pb using the Isoplot/Ex software 3.76
433 (Ludwig, 2012). The analytical uncertainties are one standard deviation (1σ), and include uncertainties
434 related to measurement and common Pb correction.

435 **5.2. Uranium–lead zircon dating results**

436 **5.2.1. Hammamat Group**

437 Sample 15-0320-06 is a pale purple quartz sandstone of the Hammamat Group. The sandstone is well
438 sorted, and is typically separated from the underlying metavolcanic rocks of the El-Dabbah Group by an
439 unconformity. The beds are weakly deformed and have a single cleavage. The sample was taken several
440 meters above the basal unconformity. One hundred and forty-five randomly selected detrital zircon grains
441 yielded ages of 1100–640 Ma, with a high proportion of younger ages (650–640 Ma) (Fig. 8A-1, A-2).
442 Three Archean grains (~2660 Ma) and one Mesoproterozoic grain (1870 Ma) were identified. The zircon
443 age distribution shows five main peaks at ~838, ~784, ~745, ~680, and ~650 Ma. The age peak at ~680
444 Ma is the largest, followed by those at ~640 and ~650 Ma. This U-Pb zircon age data is deferred to
445 Section 7.

446 **5.2.2. Ages of the intrusions**

447 Samples 16-0320-52 (Figs. 3, 4E) and 16-0320-53 (Fig. 3) are from the quartz porphyry that intrudes
448 the Atshan Formation within the NW domain. Zircons from sample 16-0320-52 yielded a mean age of
449 659.6 ± 3.0 Ma (Fig. 8C-1, C-2) and sample 16-0320-53 yielded two age peaks at ~650 and ~680 Ma
450 (Fig. 8B-1, B-2). These ages constrain the timing of the sedimentation of the Atshan Formation.
451 Sample 16-0318-45 is from a hornblende–biotite granite on the southern margin of the SW domain
452 (Figs. 3, 4G). The granite is massive, homogeneous, lacks a strong foliation (Khudeir et al., 1995), and
453 was deformed by the El-Dabbah Fault (Fig. 2). Zircons from the hornblende–biotite granite yielded a
454 mean age of 638.1 ± 2.9 Ma (Fig. 8D-1, D-2). This U-Pb zircon age data is deferred to Section 7.
455

456 **6. Sedimentary environment**

457 A reconstruction of the sedimentary environment that formed the metavolcanic–volcaniclastic
458 sequence in the CED indicates that the rocks formed in an island arc setting, based on the geochemistry of
459 the volcaniclastic rocks and granites, and the presence of ophiolitic material (e.g., El-Bialy, 2019). A
460 number of different tectonic models have been proposed to account for the north-directed subduction,

based on the characteristics of the ophiolitic material and the high-grade metamorphic complex (e.g., Loizenbauer et al. 2001; Abd El-Naby and Frisch, 2002). The rare earth element concentrations and Ti/V values are consistent with an island arc, MORB, back-arc (Ahmed et al., 2001; Farahat, 2010), or forearc setting (Abd El-Rahman et al., 2009). The composition of relict Cr-spinel in the serpentinized mantle peridotites, the high Cr contents, and high values of Mg/(Mg + Fe) in olivine indicate that the peridotites are highly depleted residual mantle, consistent with a forearc setting (Azer and Stern, 2007; Khalla and Azer, 2007).

The tectonic setting and stratigraphic characteristics of the volcano-sedimentary sequences are not well understood because these rocks are strongly deformed in many areas, so they could not be used to constrain the tectonic models. In contrast, the El-Dabbah Group is relatively low-grade and weakly deformed, so it might provide useful constraints on this sequence, which is inferred to have formed at the margins of an island arc.

In our stratigraphic reconstruction, the El-Dabbah Group is constrained by the following observations. 1) There is a total thickness of >5 km of volcanic–volcaniclastic rocks. 2) The grain size decreases upward through the sequence. The Lower ED Formation contain thick massive lavas and pillow lavas with some dolerites; the Middle ED Formation contains pillow lavas, volcaniclastic rocks, iron-rich beds that record hydrothermal activity, and accretionary lapilli. The Upper ED Formation contains altered fine-grained volcaniclastic rocks and some lava flows. This sequence is typical of the sequence of sediments deposited proximal to island arc volcanoes. The multiple pillow lavas and eruptive accretionary lapilli tuffs indicate that sedimentation occurred close to an active submarine or subaerial volcano. The iron-rich sediments, BIF, and diamictite beds within the CED volcaniclastic sequence formed during the Sturtian glaciation, and record Snowball Earth conditions (Ali et al., 2010; Stern et al., 2013; Stern, 2017). Diamictites were not observed in association with the BIF of the El-Dabbah Formation within the study area. The combination of thick layers of volcaniclastic rocks, pillow basalts, and beds of precipitated iron-rich material record hydrothermal activity and proximal volcanic activity. The proportion of material associated with island arc volcanism decreases within the upper unit. Previous dating of the volcaniclastic and metamorphic rocks of the CED indicates that island arc accretion (D_1) occurred at ~700–680 Ma (Ali et al., 2009; El-Shazly and Khalil, 2016). After volcanism, the El-Dabbah Group was exhumed during collision and thrusting, and the Atshan Formation was deposited before 660 Ma.

The Izu–Bonin–Mariana island arc provides a well-characterized example of a typical sedimentary sequence formed within a modern oceanic island arc setting, where the record of sedimentation extends back to 29 Ma in the Mariana arc and 27 Ma in the Izu–Bonin arc (e.g., Taylor, 1992; Taira et al., 1998; Ishizuka et al. 2006). Four sedimentary environments have been identified in oceanic island arc systems: trench slope (accretionary prism), forearc basin, central rift zone (e.g., Sumisu Rift; Taylor et al., 1991), and back-arc basin. Detailed seismic imaging and ODP drilling (Legs 125 and 126; Taylor et al., 1991) of these sedimentary basins of oceanic island arc system have revealed the following sedimentary features

(e.g., Taylor, 1992). Mounds of serpentinite occur on the trench slope, and these have been interpreted as forearc ophiolites. The sediments are not thick or coarse-grained, because the forearc basin traps most of the sediment derived from the oceanic island arc. The trench slope in the oceanic island arc is further in typical continental or subaerial island arcs.

The forearc basin contains a 1500-m-thick sequence of pumiceous gravels and sandstones that overlie a >200-m-thick pyroclastic sequence with andesitic lavas (ODP Leg 126, Site 793; Taylor, et al. 1992). The cyclic volcaniclastics within this basin record front- and back-arc volcanism and hydrothermal circulation (Taylor, 1992). In general, forearc basins are likely to contain mostly volcaniclastic sedimentary rocks with minor lava and intrusions.

The central rift zone is well preserved in the northern section of the Izu–Bonin arc (e.g., Smith rift; Taylor et al., 1991; Taira et al., 1998). It formed close to the volcanic front and is inferred to record the syn-rift stage of back-arc basin formation. An 800-m-thick volcano–sedimentary sequence lies above 300 m of thick basaltic lavas that include lapilli tuffs (ODP 126, Site 791; Taylor 1992). More intense periods of volcanic activity produced pumice gravels and sands that are preserved within silt- and clay-dominated hemipelagic sediment that were deposited during quiescent periods (e.g., 400 kyr, Smith rift). Hydrothermal circulation in the central rift zone is more intense than at other sites. Parts of the Smith rift basin yield heat fluxes as high as 397 mW m^{-2}, compared with 13–27 mW m^{-2} fore arc and back arc basins (Yamazaki, 1988; Taylor, 1992).

Back arc basins are well developed with the Shikoku and Mariana basins. The sediments resemble those of the central rift zone sequence during the initial stages of spreading. However, the depth of sedimentation increases after spreading is established, and hemipelagic–pelagic fine-grained sediments are deposited.

The El-Dabbah Group is most similar to the sediments of the central rift zone, based on the following observations: (1) a very thick volcano-sedimentary sequence records long-lived volcanic activity and subsidence during volcanism; (2) continuous cyclic volcanic lava flow sequences with fine-grained volcanic tuffs and thick accretionary lapilli indicate that sedimentation occurred very close to the volcanic front; and (3) the BIF within the Middle ED Formation might record hydrothermal activity within a rift valley environment. In this way, total >5 km of volcanic–volcaniclastic rocks sequence may be identified crustal section of the central rift zone of oceanic island arc succession.

7. Tectonic reconstruction

We used our new detailed observations of geological relationships and age data to reconstruct the geological and tectonic history of the El-Dabbah area, including the stratigraphy and deformation of the accreted island arc sequence. We identified four fault systems (F_1 to F_4) and three sedimentary sequences (El-Dabbah Group, Atshan Formation, and Hammamat Group) in the Wadi El-Dabbah area. We used the new zircon U–Pb age data and the reported sedimentation age of iron formation (Khalil et al., 2015; Abd

El-Rahaman et al., 2019) to recognize three stages of sedimentation (Sed 1–3), quartz porphyry and granitic magmatism, and three phases of deformation (D_1–D_3) (Fig. 9).

7.1. Stage 1

Stage 1 comprises a island arc-related volcanic sedimentation (Sed 1) and a island arc accretion (D_1). Sed 1 is recorded by the volcano–sedimentary sequence, which is inferred to have formed in an island arc setting. The island arc accretion (D_1) is recorded by thrust faulting (F_1) that caused stacking of the metavolcanic rocks and lower greenschist-facies metamorphism. This involved oblique thrusting during NW–SE-directed convergence at ~690–670 Ma (Fritz et al., 1996; Augland et al., 2012; El-Shazly and Khalil, 2016). The El-Sibai gneiss complex, which lies to the south of the El-Dabbah area, records NW-ward displacement on extension shear zones. The early stages of deformation are well preserved and involved the formation of low-angle ductile shear zones and mylonites (Fowler et al., 2007; Mohamed and El-Wahed, 2008). The accretion is also represented by the ophiolitic rocks, which were emplaced during the early stages of deformation and record NNW–SSE shortening that formed imbricate structures and a thrust nappe in the gneiss complex (Bregar et al., 2002; Mohamed and El-Wahed, 2008). After this deformation, NE-directed thrusting caused ENE–WSW compression and NE–SW oriented shortening (Bregar et al., 2002; Mohamed and El-Wahed, 2008).

In the El-Dabbah area, layer-parallel shear zones that contain asymmetric folds and record top-to-the-south shearing small scale thrust faults are partially identfied, but the stratigraphy of the volcaniclastic sequence is still relatively well preserved. The lower boundary of the autochthon within this volcaniclastic sequence is not preserved. However, a top-to-the-south displacement is inferred from asymmetric folds and shear zones within NNE-dipping beds, consistent with movement of the footwall (southern domain) toward the NNE. These structures record an opposite sense of movement to the F_2 normal faults. Mohamed and El-Wahed (2008) also reported NNW–SSE shortening followed by NE–SW compressional deformation related to NE-directed thrusting in the El-Dabbah area. This structure might be related the NE-SW compressional deformation with NE dipping subduction sense.

7.2. Stage 2

Stage 2 involved the intrusion of granites, regional sedimentation in a transtensional setting, and deformation related to continental stabilization after island arc accretional deformation. In the area around the El-Sibai gneiss complex, NW–SE-trending extension formed low-angle normal ductile shear zones and mylonites after the early stages of nappe formation (Fowler et al., 2007; Mohamed and El-Wahed, 2010). This extension is roughly contemporary to NW–SE-oriented strike-slip shearing during the early stages of movement on the Najd fault system at 660–580 Ma.

Stage 2 is subdivided three events: (1) sedimentation of the Atshan Formation (Sed 2), (2) intrusion of porphyritic granites, and (3) NNE–SSE-oriented extension (D_2). The first event involved sedimentation of the Ashtan Formation (Sed 2) in a shallow water setting. This formation includes debris flows, conglomerates, angular volcanic pebbles within a muddy matrix, and fluvial–lacustrine sediments. We

infer that these rocks were deposited in a subaerial sedimentary basin proximal to mountains that were undergoing active uplift and erosion. The Sed 2 event might record the early stages of crustal stabilization after island arc accretion, in which case the sedimentary basin can be thought of as a collision-related molasse basin that formed during the mountain building phase, at the same time as transpressional deformation within the El-Sibai shear zone.

In the second event, quartz porphyry intruded in the Atshan Formation along the NW domain at 660–650 Ma. Deposition of the Atshan Formation is constrained to ~680–660 Ma, and the granites intruded the SE and SW domains at ~630 Ma.

The third event, D_2, involved two types of faulting, F_2 and F_3. The F_2 normal faulting is represented in the El-Dabbah area by a N- to NNE-dipping normal fault. Faults that formed during this event trend WNW–ESE and divide the El-Dabbah Group into northern and southern domains. The strike of the F_2 faults is sub-parallel to the stretching direction recorded by the El-Sibai gneiss complex (Fig. 3).

The boundary between the NE domain of the El-Dabbah Group and the Atshan Formation is a NNE side-down normal F_2 fault that records overlapping sinistral shearing on northwest trend which might be affected later stage strike-slip deformation. A weakly-foliated quartz porphyry (659.6 ± 3.0 Ma) intrudes the boundary and is considered to be syn-deformation. Therefore, the regional silicic magmatism is related to crustal extension at ~660–638 Ma (e.g., Johnson et al., 2011).

The El-Dabbah Fault (F_3) is a sinistral displacement on north-south fault that runs through the Wadi El-Dabbah. It cuts the hornblende–biotite granite (638 ± 2.9 Ma) and joins the F_2 boundary fault that separates the El-Dabbah and Atshan formations. The N–S orientation might record transtension during the extension recorded by the El-Sibai gneiss complex. We infer that the El-Dabbah Fault (F_3) and the NNE side down normal faults (F_2) are transtensional transfer faults that formed while the El-Sibai shear zone was active, and prior to sedimentation of the Hammamat Group (Fig. 10).

It is plausible that the different stratigraphic thickness of the Middle ED Formation within the SW and SE domains is related to extensional normal faulting (F_2) and sinistral movement on the El-Dabbah Fault (F_3). Extension related to the normal faulting is more pronounced in the NE and SE domains than in the NW and SW domains (Fig. 10). The south end of the SE domain is situated to the north of the El-Sibai gneiss complex and is more strongly foliated than the SW domain. Therefore, it might represent deeper parts of the crust than the SW domain. If the SE domain experienced more exhumation than the SW domain, then truncation of normal faults within the middle of the Middle ED Formation might explain why the Middle ED Formation is thinner in the SE domain than in the SW domain (Fig. 10).

These regional transtensional deformation at ~638–600 Ma was associated with early activity on the El-Sibai shear zone and might have been related to movement on the regional Najd fault system elsewhere on the Arabian shield (Fig. 1; Fritz et al., 1996; Abd El-Wahed et al., 2007, 2008, 2010; Fowler et al., 2007). The regional transtensional deformation might have been related to crustal thickening

associated with granitic intrusion in the East African Orogeny (e.g., Stern, 1985; Shalaby et al., 2006; Abd El-Wahed, 2010, Fritz et al., 2013).

7.3. Stage 3

Stage 3 can be divided into two sub-stages: Hammamat Group sedimentation (Sed 3) and transtentional deformation (D_3). Sed 3 in the El-Dabbah area involved the formation of the ~12 -kilometer-wide Kareim basin, which preserves a >8000-m-thick section of the subaerial Hammamat Group sediments (Fritz et al., 1996). The Kareim basin experienced two periods of deformation (Abd El-Wahed, 2007). The first period involved the formation of NW and SE sides down -normal faults in response to orogen-parallel extension and the generation of granitic magmas intruded in the Sibai metamorphic complex at ~650 ± 10 Ma (Fritz and Messner, 1999; Abd El-Wahed, 2007). The second period involved regional sinistral NW–SE-oriented shearing on the Najd fault system, and the development of a pull-apart regime in response to NNW–SSE-oriented tensional stress. Pebbles sequence within the conglomerates are identified at the upper part of the sequence which source come from the strike-slip transpressional mountain building event (Fritz and Messner, 1999, Mohamed and El-Wahed, 2010).

In the El Dabbah area, the Hammamat Group occurs on hilltops and above a well-preserved unconformity. Sandstones with occasional pebbles commonly occur on the contact. The absence of a thick basal conglomerate indicates that this group might have formed toward the center of the sedimentary basin.

The D_3 is represented by NNE-side-down normal faults (F_4) within the NE and NW domains. The F_4 faults are ten-meter-scale displacement with the Hammamat Group, recording NNE-SSW extension. The F_4 faults formed during the first period of deformation that is recorded on the southern margin of the Kareim basin (Fritz and Messner, 1999, Mohamed and El-Wahed, 2010). Strong NW–SE-trending strike-slip deformation was reported the north side of the Hammamat Basin and the El-Sibai shear zone (Fritz and Messner, 1999). F_4 faults may be related as transtension deformation of this strike-slip deformation.

The detrital zircon U–Pb age spectra of sandstones from the lower parts of the Hammamat Group in the El-Dabbah area show a peak at 680 Ma and minimum ages of 650–640 Ma. These ages are similar to the crystallization age of the quartz porphyry that intrudes the Atshan Formation (660–650 Ma). Therefore, the Hammamat Group was deposited after intrusion of the quartz porphyry (660–650 Ma). Detrital zircon age spectra of other Hammamat Group samples also show peaks at 680 and 650 Ma (Wilde and Youssef, 2002), and detrital zircons from samples of the Hammamat Group from the North Eastern Desert yield a mean age of 585 ± 13 Ma, consistent with a Dokhan volcanic rock source (Wilde and Youssef, 2002). However, the sample from the basal sequence exposed in the southern Kareim basin does not yield 585 Ma zircons. Therefore, it is likely that 680 and 650 Ma granitic rocks were exposed in the Eastern Desert, that these rocks were not affected by the Dokhan volcanic activity, and that deposition of the Hammamat Group began at ~620–590 Ma in this area. The D_3 sub-stage might be equivalent to the

640 syn-sedimentary deformation related to the formation of the Kareim basin that occurred after
641 sedimentation of the Hammamat Group and after ~580 Ma.
642 In our reconstruction, strike-slip deformation continued for an extended period subsequent to
643 accretion of the island arc sequence. The Atshan Formation was deposited within a collision-related
644 transpressional strike-slip sedimentary basin, and the Hammamat Group was deposited in a continental
645 strike-slip basin formed by continuous strike-slip transtentional deformation, which might have been
646 related to orogenic collapse after the East African Orogeny (Fig. 9; Stern and Johnson, 2010; Johnson et
647 al., 2011).
648
649 **8. Conclusions**
650 1) Three stratigraphic units were defined in the Wadi El-Dabbah area, based on detailed mapping:
651 the El-Dabbah Group (~770–700 Ma), the Atshan Formation (~680–650 Ma), and the Hammamat
652 Group (~620–580 Ma). The hornblende–biotite granite intruded the El-Dabbah Group at 638 Ma
653 and the quartz porphyry intruded the Atshan Formation at 650–640 Ma.
654 2) The El-Dabbah Group consists of >7500 m of well-preserved volcano-sedimentary rocks. The
655 group was divided into three formations. The Lower ED Formation consists of massive coarse-
656 grained metavolcanic rocks and thin volcaniclastic sequences. The Middle ED Formation
657 comprises basaltic massive rocks, pillow lavas, and volcaniclastic rocks, with thinly bedded iron-
658 rich beds and greenish-black shales. The Upper ED Formation consists of a fine volcaniclastic
659 sedimentary sequence. The very thick volcaniclastic sequences, the fining upward and massive
660 volcanics to fine volcaniclastic stratigraphy are identified as this sequence are formed a shallow
661 portion of crustal section of a intra arc central rift zone associated with an oceanic island arc.
662 3) The Atshan Formation consists of subaerially deposited sedimentary rocks, including debris flow
663 conglomerates and a sandstone and shale sequence with lacustrine varves. Deposition occurred
664 prior to deposition of the Hammamat Group. This formation may have been deposited as a
665 collision-related sedimentary basin that formed during the mountain building phase
666 transpressional deformation.
667 4) Three stages of sedimentation and deformation were recognized, based on structural observations,
668 stratigraphic relationships, and the ages of the granitic intrusions.
669 Stage 1 was characterized by the El-Dabbah Group deposited within island arc-related
670 volcano–sedimentary sequence (Sed 1) and it affected thrust deformation (D_1). This stage was
671 related to sedimentation and accretion of the oceanic island arc. The El-Dabbah Group was
672 affected by top-to-the-south low angle thrusting during accretion.
673 Stage 2 involved sedimentation of the Atshan Formation and deformation with NW–SE-
674 trending transtension, N-dipping normal faulting (F_2), and N–S-trending strike-slip faulting (F_3)
675 which related the El Sibai shear zone. This stage was associated with movement on the Najd

fault system elsewhere on the Arabian Shield and regional deformation. Deformation was also associated with exhumation of high-grade mid-crustal core complexes and plutonic rocks. Depositional timing of the Atshan Formation are early stages of crustal stabilization during the collisional stages of the East African Orogeny, which involved oblique transpressional convergence of the northern parts of east and west Gondwana.

Stage 3 involved sedimentation of the Hammamat Basin and transtensional deformation of strike-slip deformation of continuous active of the El Sibai shear zone. This stage might have been related to orogenic collapse after the East African Orogeny.

Acknowledgements

This study was supported by Grants-in-Aid from the Japanese Ministry of Education, Culture, Sports, Science, and Technology (22253008 and 26257211). We thank you to Abd El-Mahed, H. Fritz and A. Kamal for very detail reviews and helpful comment to this paper. We acknowledge the assistance of the 2016 short term research dispatch–invite program of Kyushu University, Japan, and the Kochi Core Center, Japan. This study was performed in collaboration with the Center for Advanced Marine Core Research (CMCR) of Kochi University, Japan (13A002, 13B002, 14A009, 14B007, 15A050, 15A045, 16A038, 16B034, 17A002, and 17B002) and the research program of Menoufiya University, Egypt.

References

Abdeen, M.M., and Abdelghaffar, A.A., 2011. Syn- and post-accretionary structures in the Neoproterozoic Central Allaqi-Heiani suture zone, Southeastern Egypt. Precambrian. Research, 185, 95–108.

Abd El-Naby, H.H., and Frisch, W., 2002. Origin of the Wadi Haimur–Abu Swayel gneiss belt, south Eastern Desert, Egypt: petrological and geochronological constraints. Precambrian. Research, 113, 307–322.

Abd El-Rahman, Y., Polat, A., Dilek, Y., Fryer, B.J., El-Sharkawy, M., Sakran, S., 2009. Geohemistry and tectonic evolution of the Neoproterozoic incipient arc-fore-arc crust in the Fawakhir area, Central Eastern Desert of Egypt. Precambrian Research, 175, 116–134.

Abd El-Rahman, Y., Gutzmer, J., Li, X.H., Seifert T., Li, C.F., Ling, X.X., Li, J., 2019. Not all Neoproterozoic iron formations are glaciogenic: Sturtian-aged non-Rapitan exhalative iron formations from the Arabian–Nubian Shield. Mineralium Deposita. 1-20, Online. https://doi.org/10.1007/s00126-019-00898-0

Abd El-Wahed, M.A., 2007. Pan-African strike-slip tectonics of Wadi El-Dabbah area, north Sibai Core Complex, Central Eastern Desert, Egypt. Annals of the Egyptian Geological Survey, 29, 1–36.

Abd El-Wahed, M.A., 2008. Thrusting and transpressional shearing in the Pan-African nappe southwest El-Sibai core complex, Central Eastern Desert, Egypt. Journal of African Earth Sciences, 50, 16–36.

Abd El-Wahed, M.A., 2010. The role of the Najd Fault System in the tectonic evolution of the Hammamat molasse sediments, Eastern Desert, Egypt. Arabian Journal of Geosciences, 3, 1–26.

Abd El-Wahed, M.A., Lebda, E., Ali, A., Kamh, S., and Attia, M., 2019. The structural geometry and metamorphic evolution of the Umm Gheig shear belt, Central Eastern Desert, Egypt: Implications for exhumation of Sibai Core Complex during oblique transpression. Arabian Journal of Geosciences 12: 764.

Abdelsalam, M.G., and Stern, R.J., 1996. Sutures and shear zones in the Arabian-Nubian shield. Journal of African Earth Sciences, 23, 289–310.

Ali, K.A., Stern, R.J., Manton, W.I., Kimura, J.-I., Khamees, H.A., 2009. Geochemistry, Nd isotopes and U-Pb SHRIMP zircon dating of Neoproterozoic volcanic rocks from the Central Eastern Desert of Egypt: new insights into the ~750 Ma crust-forming event. Precambrian. Research, 171, 1–22.

Ali, K.A., Stern, R.J., Manton, W.I., Johnson, P.R., Mukherjee, S.K., 2010. The Neo-proterozoic Atud Diamictite of the Eastern Desert of Egypt and Northern Saudi Arabia: evidence of ~750 Ma glaciation in the Arabian-Nubian Shield?, International Journal of Earth Sciences 99, 705–726.

Ahmed, A.H., Arai, S., Attia, A.K., 2001. Petrological characteristics of podiform chromitites and associated peridotites of the Pan African ophiolite complexes of Egypt. Mineralium Deposita, 36, 72–84.

729 Augland, L.E., Andresen, A., Boghdady, G.Y., 2012. U-Pb ID-TIMS dating of igneous and
730 metaigneous rocks from the El-Sibai area: time constraints on the tectonic evolution of the Central
731 Eastern Desert, Egypt. International Journal Earth Science, 101, 25–37.
732 Azer, M.K., Stern, R.J., 2007. Neoproterozoic (835–720 Ma) serpentinites in the Eastern Desert,
733 Egypt: fragments of fore-arc mantle. Journal of Geology, 115, 457–472.
734 Basta, F.F., Maurice, A.E., Fontbote L., Favarger P.Y., 2011. Petrology and geochemistry of the
735 banded iron formation (BIF) of Wadi Kareim and Um Anab, Eastern Desert, Egypt: Implications for the
736 origin of Neoproterozoic BIF. Precambrian. Research, 187, 277–292.
737 Bezrnjani R.N., Pease V., Whitehouse M.J., Shalaby M.H., Kadi K.A., Kozdroj W., 2014. Detrital
738 zircon geochronology and provenance of the Neoproterozoic Hammamat Group (Igla Basin), Egypt and
739 the Thalbah Group, NW Saudi Arabia: Implications for regional collision tectonics. Precambrian.
740 Research, 245, 225–243.
741 Black L.P., Kamo S.L., Allen C.M., Davis D.W., Aleinikoff J.N., Valley J.W., Mundil R., Campbell
742 I.H., Korsch R.J., Williams I.S., Foudoulis C., 2004. Improved 206Pb/238U microprobe geochronology
743 by the monitoring of a trace-element-related matrix effect; SHRIMP, ID-TIMS, ELA-ICP-MS and
744 oxygen isotope documentation for a series of zircon standards. Chemical Geology, 205, 115–140.
745 Bregar, M., Bauernhofer, A., Pelz, K., Kloetzli, U., Fritz, H., Neumayr, P., 2002. A late
746 Neoproterozoic magmatic core complex in the Eastern Desert of Egypt; emplacement of granitoids in a
747 wrench-tectonic setting. Precambrian. Research, 118, 59–82.
748 Cawood, P.A., 2005. Terra Australis Orogeny: Rodinia breakup and development of the Pacific and
749 Iapetus margins of Gondwana during the Neoproterozoic and Paleozoic. Earth Science Reviews. 69, 249–
750 279.
751 Claoué-Long, J.C., Compston, W., Roberts, J., Fanning, C.M., 1995. Two Carboniferous ages: a
752 comparison of SHRIMP zircon dating with conventional zircon ages and 40Ar/39Ar analysis. In:
753 Berggren, W.A., Kent, D.V., Aubrey, M.P., Hardenbol, J. (Eds.), Geochronology, Time Scales and
754 Global Stratigraphic Correlation. Society for Sedimentary Geology Special Publication, 54, 3–21.
755 EGSMA (Egyptian Geological Survey and Mining Authority), 1996. Geological map of Wadi
756 Jabjahah Quadrangle, Egypt, Scale 1:250.000. Egyptian Geological Survey and Mining Authority, Cairo,
757 Egypt
758 EGSMA, 2002. Geological Map of Marsa Shaab Quadrangle, Egypt at Scale 1:250,000. Egyptian
759 Geological Survey and Mining Authority, Cairo, Egypt
760 El-Bialy, M.Z., 2019. Precambrian basement complex of Egypt. In: Hamimi Z., El-Barkooky A., Frias
761 J.M., Fritz H., El-Rahman A.E., (Eds), The geology of Egypt, 38-80, Springer Nature, Switzerland.
762 El-Gaby, S. El-Nady O., Khudeir A., 1984. Tectonic evolution of the basement complex in the central
763 eastern desert of Egypt. International Journal of Earth Sciences, Geologische Rundschau, 73, 3, 1019–
764 1036.

765 El-Ramly, M. F., 1972. A new geological map for the basement rocks in the Eastern and
766 Southwestern Deserts of Egypt. Annual report of Geological Survey Egypt, 2, 1–18.
767 El-Shazly A.K., and Khalil K.I., 2016. Metamorphic and geochronologic constraints on the tectonic
768 evolution of the Central Eastern Desert of Egypt. Precambrian. Research, 283, 144-168.
769 Farahat E.S., 2010. Neoproterozoic arc–back-arc system in the Central Eastern Desert of Egypt:
770 evidence from supra-subduction zone ophiolites. Lithos, 120, 293–308.
771 Fowler, T. J., Osman, A. F., 2001. Gneiss-cored interference dome associated with two phases of late
772 Pan-African thrusting in the central Eastern Desert, Egypt. Precambrian. Research, 108, 1-2, 17-43.
773 Fowler, A.R., Khamees, H., Dowidar, H., 2007. El Sibai gneissic complex, Central Eastern Desert,
774 Egypt: folded nappes and syn-kinematic gneissic granitoid sheets -not a core complex. Journal of African
775 Earth Sciences, 49, 4, 119–135.
776 Fowler, T. J., and Osman, A. F., 2013. Sedimentation and inversion history of three molasse basins of
777 the western Central Eastern Desert of Egypt: Implications for the tectonic significance of Hammamat
778 basins. Gondwana Research. 23, 1511-1534.
779 Fowler, A.R., and Hamimi, Z., 2020. Structural and Tectonic Frame work of Neoproterozoic
780 Basement of Egypt: From Gneiss Dome to Transpression Belts. In: Hamimi Z., El-Barkooky A., Frias
781 J.M., Fritz H., El-Rahman A.E., (Eds), The Geology of Egypt, Regional Geology Reviews, 81-123,
782 Springer Nature, Switzerland.
783 Fritz, H., Wallbrecher, E., Khudier, A.A., Abu El-Ela, F., Dallmeyer, R.D., 1996. Formation of
784 Neoproterozoic metamorphic core complexes during oblique convergence, Eastern Desert, Egypt. Journal
785 of African Earth Sciences, 23, 311–329.
786 Fritz H., and Messner M., 1999. Intramontane basin formation during oblique convergence in the
787 Eastern Desert of Egypt: magmatically versus tectonically induced subsidence. Tectonophysics, 315, 145-
788 162.
789 Fritz H., Dallmeyer D.R., Wallbrecher E, Loizenbauer J, Hoinkes G., Neumayr P., Khudeir A.A.,
790 2002. Neoproterozoic tectonothermal evolution of the Central Eastern Desert, Egypt: a slow velocity
791 tectonic process of core complex exhumation. Journal of African Earth Sciences, 34, 137-155.
792 Fritz H., Abdelsalam M., Ali K.A., Bingen B., Collins A.S., Fowler A.R., Ghebreab W.,
793 Hauzenberger C.A., Johnson P.R., Kusky T.M., Macey P., Muhongo S., Stern R.J., Viola G., 2013.
794 Orogen styles in the East African Orogen: A review of the Neoproterozoic to Cambrian tectonic
795 evolution. Journal of African Earth Sciences, 86, 65-106.
796 Hamdy, M.H., El-Wahed, M.A., Abd El-Dien, H.G., Morishita, T., 2017. Garnet hornblendite in the
797 Meatiq Core Complex, Central Easter Desert of Egypt: Implications for crustal thickening preceding the
798 76 M. Z. El-Bialy 600 Ma extensional regime in the Arabian-Nubian Shield. Precambrian Research, 298,
799 593–614.

Hamimi Z., Abd El-Wahed M.A., Gahlan H.A. and Kamh S. Z., 2019. Tectonics of the Eastern Desert of Egypt: Key to Understanding the Neoproterozoic Evolution of the Arabian–Nubian Shield (East African Orogen). In: Bendaoud A., Hamimi Z., Hamoudi M., Djemai S., Zoheir B., (eds) Geology of the Arab world—an overview. Springer Geology, pp 1–81.

Hamimi Z., Abd El-Wahed M.A., 2020. Suture(s) and Major Shear Zones in the Neoproterozoic Basement of Egypt. In: Hamimi Z., El-Barkooky A., Martínez Frías J., Fritz H., Abd El-Rahman Y. (eds) The Geology of Egypt. Regional Geology Reviews. Springer, 153–189.

Hassan, S.H., El kazzaz, Y.A., Taha M.M.N., Mohammad A.T., 2017. Late Neoproterozoic basement rocks of Meatiq area, Central Eastern Desert, Egypt: Petrography and remote sensing characterizations. Journal of African Earth Sciences, 131, 14-31.

Horie K., Takehara M., Suda Y., Hidaka H., 2013. Potential Mesozoic reference zircon from Unazuki plutonic complex: geochronological and geochemical characterization. Island Arc, 22, 292–305.

Ishizuka, O., Kimura, J., Li, Y.B., Stern, R.J., Reagan, M.K., Taylor,R.N., Ohara,Y., Bloomer, S.H., Ishii, T., Hargrove III, U.S., Haraguchi S., 2006, Earth and Planetary Science Letters, 250, 385–401

Johnson, P.R., 2014, An Expanding Arabian-Nubian Shield Geochronologic and Isotopic Dataset: Defining Limits and Confirming the Tectonic Setting of a Neoproterozoic Accretionary Orogen. The Open Geology Journal, 2014, 8, 3-33.

Johnson, P.R., and Woldehaimanot, B., 2003. Development of the Arabian- Nubian Shield: perspectives on accretion and deformation in the northern East African Orogen and the assembly of Gondwana, in: Yoshida, M., Windley, B.F., Dasgupta, S. (Eds.), Proterozoic East Gondwana: Supercontinent Assembly and Breakup, Geological Society, London, Special Publication 206, 289–325.

Johnson, P.R., Andresen A., Collins A.S., Fowler A.R., Fritz H., Ghebreab W., Kusky T., Stern R.J., 2011. Late Cryogenian-Ediacaran history of the Arabian-Nubian Shield: A review of depositional, plutonic, structural, and tectonic events in the closing stages of the northern East African Orogen. Journal of African Earth Sciences, 61, 167–232.

Khalil, A.E.S., Azer, M.K., 2007. Supra-subduction affinity in the Neoproterozoic serpentinites in the Eastern Desert, Egypt: Evidence from mineral composition. Journal African Earth Science, 49, 136–152.

Khalil K.I., El-Shzly A.E., Lehmann B., 2015. Late Neoproterozoic banded iron formation (BIF) in the central Eastern Desert of Egypt: Mineralogical and geochemical implications for the origin of the Gebel El Hadid iron ore deposit. Ore Geology Reviews, 69, 380-399.

Khudeir, A.A., El-Gaby S., Kamal El-Din, G., Asran, A.M.H., Greiling R.O., 1995. The pre-Pan-African deformed granite cycle of the Gabal El-Sibai swell, Eastern Desert, Egypt. Journal of African Earth Sciences, 21, 396–406.

Kiyokawa, S., 1992. Geology of the Idonnappu Belt, central Hokkaido, Japan: Evolution of a Cretaceous Accretionary Complex. Tectonics, 11, 6, 1180-1206.

Loizenbauer, J., Wallbrecher, E., Fritz, H., Neumayr, P., Khudeir, A.A., Kloetzli, U., 2001. Structural geology, single zircon ages and fluid inclusion studies of the Meatiq metamorphic core complex: Implications for Neoproterozoic tectonics in the Eastern Desert of Egypt. Precambrian Research, 110, 357–383.

Ludwig, K.R., 2009. SQUID 2: a user's manual, Berkeley Geochronology Center Special Publication, Berkeley, 2, 104p

Ludwig, K.R., 2012. Isoplot 3.75-4.15: A geochronological toolkit for Microsoft Excel, Berkeley Geochronology Center Special Publication, Berkeley, California.

Maurice, A.E., 2000. Petrology and mineralization of Gebel Abu Marawat area, Eastern Desert, Egypt. M.Sc. thesis, Cairo University, 226 p.

Meert, J.G., 2003. A synopsis of events related to the assembly of Eastern Gondwana. Tectonophysics, 362, 1–40.

Neumayr, P., Moinkes, A., Hoinkes, G., Puhi, J., 1996. Geological setting of the Meatiq metamorphic core complex: petrological and geological evidence. Journal of African Earth Sciences, 23, 3, 331-345.

Neumayr, P., Hoinkes, G., Puhi, J., Mogessie, A., Khudeir, A.A., 1998. The Meatiqu dome (Eastern Desert, Egypt) a Precambrian metamorphic core complex: petrological and geological evidence. Journal of Metamorphic Geology, 16, 259-279.

Paces, J.B., Miller J.D., 1993. Precise U–Pb ages of Duluth Complex and related mafic intrusions, northeastern Minnesota: Geochronological insights to physical, petrogenetic, paleomagnetic, and tectonomagmatic processes associated with the 1.1 Ga Midcontinent Rift System. Journal Geophysical Research, 98, 13997–14013.

Shalaby, A., Stüwe, K., Makroum, F., Frtiz, H., Kebede, T., Klötzli, U., 2005. The Wadi Mubarak belt, Eastern Desert of Egypt: a Neoproterozoic conjugate shear system in the Arabian–Nubian Shield. Precambrian. Research, 136, 27–50.

Shalaby, A., Stüwe, K., Fritz, H., & Makroum, F., 2006. The El Mayah molasse basin in the Eastern Desert of Egypt. Journal of African Earth Sciences, 45, 1, 1-15.

Stacey, J.S., Kramers, J.D., 1975. Approximation of terrestrial lead isotope evolution by a two-stage model. Earth and Planetary Science Letters, 26, 207–221.

Stein, M., Goldstein S.L., 1996. From plume head to continental lithosphere in the Arabian-Nubian Shield. Nature, 382, 773–778.

Stein, M., 2003.Tracing the plume material in the Arabian-Nubian Shield. Precambrian Research, 123, 223–234.

Stern R.A., Bodorkos S., Kamo S.L., Hickman A.H. and Corfu F., 2009. Measurement of SIMS instrumental mass fractionation of Pb-isotopes during zircon dating. Geostandards and Geoanalytical Research, 33, 145–168.

Stern R.J., 1985. The Najd Fault system, Saudi Arabia and Egypt: a Late Precambrian rift-related transform system? Tectonics, 4. 497-511.

Stern, R.J., 1994. Arc assembly and continental collision in the Neoproterozoic East African Orogeny: implications for the consolidation of Gondwanaland. Annual Review Earth Planetary Science, 22, 319–351.

Stern R.J., 2017. Neoproterozoic formation and evolution of Eastern Desert continental crust—the importance of the infrastructure- superstructure transition. Journal of African Earth Sciences, 146, 15-27.

Stern, R.J., and Hedge, C.E., 1985. Geochronologic and isotopic constraints on late Precambrian crustal evolution in the Eastern Desert of Egypt. American Journal of Science, 285, 2, 97-127.

Stern, R.J., Johnson, P.J., Kröner, A., Yibas, B., 2004. Neoproterozoic ophiolites of the Arabian–Nubian Shield, in: Kusky, T. (Ed.), Precambrian Ophiolites. Elsevier, pp. 95–128.

Stern, R.J., and Johnson, P.J., 2010. Continental lithosphere of the Arabian Plate: A geologic, petrologic, and geophysical synthesis. Earth Science Reviews, 101, 29-67.

Stern, R.J., Mukherjee, S.K., Miller, N.R., Ali, K., Johnson, P.R., 2013. ~750 Ma banded iron formation from the Arabian-Nubian Shield—Implications for understanding neoproterozoic tectonics, volcanism, and climate change. Precambrian. Research, 239, 79– 94.

Tadesse, T., Hoshino, M., Sawada, Y., 1999. Geochemistry of low-grade metavolcanics rocks from the Pan-African of the Axum area, northern Ethiopia. Precambrian. Research, 96, 101–124.

Taira A., Saito S., Aoike K., Morita S., Tokuyama H., Suyehiro K., Takahashi N., Shinohara M., Kiyokawa S., Naka J. and Klaus A., 1998. Nature and growth rate of the northern Izu-Ogasawara arc crust and their implications to continental crust formation. The Island Arc, 7, 395-407.

Taylor, B., Klaus, A., Brown, G. R., Moore, G. E, Okamura, Y, and Murakami, E, 1991. Structural development of Sumisu Rift, Izu-Bonin Arc. Journal of Geophysical Research, 96:16,113-16,129.

Taylor, B., 1992. Rifting and the volcanic–tectonic evolution of the Izu–Bonin–Mariana Arc, in: B. Taylor, K. Fujioka, et al., (Eds.), Proceedings of the Ocean Drilling Program, Scientific Results, 126, Ocean Drilling Program, College Station, TX, 627-650.

Yamazaki, T,, 1988. Heat flow in the Sumisu Rift, Izu-Ogasawara (Bonin) Arc. Bulletin of Geological Survey Japan, 39, 63-70.

Veevers, J.J., 2003. Pan-African is Pan-Gondwanaland: oblique convergence drives rotation during 650–500 Ma assembly. Geology, 31, 501–504.

Wilde S., Youssef K., 2000. Significance of SHRIMP U-Pb dating of the imperial porphyry and associated Dokhan Volcanics, Gebel Dkhan, north Eastern Desert, Egypt. Journal of African Earth Sciences, 31, 2, 403-413.

Wilde S., Youssef K., 2002. A re-evaluation of the origin and setting of the Late Precambrian Hammamat Group based on SHRIMP U–Pb dating of detrital zircons from Gebel Umm Tawat, North Eastern Desert, Egypt. Journal of the Geological Society of London, 159, 595–604.

Williams, I.S., 1998. U–Th–Pb geochronology by ion microprobe. In: McKibben, M.A., Shanks III, W.C., Ridley, W.I. (Eds.), Applications of Microanalytical Techniques to Understanding Mineralizing Processes. Reviews in Economic Geology, 7, 1–35.

Woldehaimanot, B., 2000. Tectonic setting and geochemical characterisation of Neoproterozoic volcanics and granitoids from the Adobha Belt, northern Eritrea. Journal of African Earth Sciences, 30, 4, 817–831.

Figure Captions

Fig. 1 A. Tectonic map of Afro-Arabia modified after Johnson et al. (2011) and superimposed on a Google Maps image. The white rectangle indicates the location of the geological map on the left.

1 B. Simplified geological map of the Nubian Shield, North and Central Eastern Desert, Egypt (after Basta et al., 2011). The black rectangle shows more detail map at Fig. 2. Modified after EGSMA (1996, 2002) 1:250,000 Geological Map series, Johnson et al. (2011) and Hamimi and Abd El-Wahed (2019).

Fig. 2. Simplified geological map of part of the Central Eastern Desert, Egypt (modified after El-Ramly, 1972, Fowler et al., 2007, Fritz et al., 2002, Augland et al., 2012, Hamdy et al., 2013, Hassan et al., 2017). The rectangle potion indicates the location of the geologic map in Fig. 3.

Fig. 3. Geological map of the Wadi El-Dabbah area superimposed on an image from Google Earth map of 2011 version. RW and RE indicate the dry gorge branch names mentioned in the text and figure captions (e.g., RW 12). Right image from map shows N–S cross-section of the NW and SW domains. Scale of the cross-section is same as map. See 90º clockwise rotation.

Fig. 4.

A) Overview, looking east from Wadi El-Dabbah, of the well-stratified upper sedimentary sequence of Middle ED Formation, SE domain, on the eastern side of Wadi El-Dabbah, northern part of the SE domain. F_1 thrust faults cut a volcaniclastic sequence within the El-Dabbah Group. The small-scale thrust faults are sub-parallel to bedding. A N-dipping normal fault is visible in hilltop on the left of the image. The scale is shown by the car on the right hand side of the image, indicated by the arrow.
B) Overview, looking north, of layer sub-parallel isoclinal tight folding within the BIF at RW8, Middle ED Formation, SW domain. The fold axes are E–W-oriented and the asymmetry is top-to-the-south. The fault plane is sub-parallel to the shallowly N-dipping bedding. The cliff face is oriented E–W.
C) North-dipping normal fault with an unknown displacement observed in cliff sections at Wadi El-Dabbah between RE 3 and RE 4, Upper ED Formation, NW domain. Looking west from Wadi El-Dabbah. The rectangle indicates the location of Fig. 4D.
D) Close-up of the N-dipping normal fault (Fig. 4C), NW domain, looking west. The beds in the hanging-wall were dragged to the north on the fault. The well-preserved fault plane contains N-dipping slickensides with normal direction several slip steps. Sub-horizontal volcaniclastic rocks in the hanging wall overlie the bedding in the footwall, which dips to the N at 50°–60°. The hanging wall volcanics beds also bended to downside. Hanging beds move down to north side.
E) Fault (F_4) in a valley on the boundary between the Atshan Formation and the eastern margin of the NE domain. Looking southeast. The quartz porphyry (sample 16-0320-52) crops out within this

valley. The El-Dabbah and Atshan formations and quartz porphyry are on the right and left, respectively.

F) Steeply dipping N–S-trending iron formation of the Middle ED Formation on the El-Dabbah Fault, between RE 4 and RE 5 on the east side of Wadi El-Dabbah, SE domain. Looking southeast in the Wadi El-Dabbah..

G) Massive hornblende–biotite granite (sample 16-0318-45), SW domain. The granite is bounded by the southern El-Dabbah Group. The granite is not affected by strong shear deformation and is truncated by the N–S-trending El-Dabbah Fault. Looking southeast of small gouge in the granite hill.

Fig. 5. Stratigraphic and structural features of the metavolcanic–volcaniclastic sequence of the El-Dabbah Group.

A) Stratified sequence of less-deformed massive metavolcanic rocks and pillow lavas above a sub-horizontal volcaniclastic sequence, Upper ED Formation, near RE 01, Wadi El-Dabbah, NE domain, looking north at entrance of the RE-01.

B) Coarse-grained massive volcanic rocks (microgabbro) of the Lower ED Formation, RE 11, SE domain.

C) Well-preserved pillow basalts of the Upper ED Formation, RE 5, Wadi El-Dabbah, SE domain. View to northeast along Wadi El-Dabbah.

D) Well-preserved unconformity at the top of a hill above the volcaniclastic sequence, between RW 1 and RW 2, NW domain. Looking west at upper most part of the hill cliff along Wadi El-Dabbah.

E) Accretionary lapilli beds within a fine tuff sequence within the Middle ED Formation, RW 7, SW domain. Looking northwest.

F) Well-bedded greenish shale with graded bedding, younging to the northwest, Middle ED Formation, near RW 7, Wadi El-Dabbah, SW domain. Looking northeast.

G) Iron formation within the volcaniclastic sequence, Middle ED Formation, near RW7, Wadi El-Dabbah, SW domain. Looking southwest along Wadi El-Dabbah.

H) Pillow lava sequence (>30 m thick), Middle ED Formation, middle of RW6, SW domain. Looking southwest at the small branch or RW6.

Fig. 6. Composite stratigraphic column of the Wadi El-Dabbah area (left), and a more detailed stratigraphic column of the SW domain (right). Gray bars with numbers preceded by ‘RW’ and ‘RE’ show the locations of the western and eastern branch gorges that lead into Wadi El-Dabbah. The locations of the wadi branches are shown on Fig. 3.

Fig. 7. Sedimentary rocks of the Atshan Formation and the Hammamat Group.

A) Overview of the Atshan Formation on the western margin of the El-Dabbah Group, SW domain. The lower parts are poorly sorted sandstones and mudstones. The upper boundary is a basaltic dike (orange rock in the photograph). Hilltops in this area commonly expose the unconformity that separates the Atshan Formation from the sandstones and conglomerates of the Hammamat Group. View to northeast along wadi.

B) Close-up view of muddy matrix-supported conglomerate. The clasts are poorly sorted and include angular–subangular green and black volcanic rocks. View to east along wadi cliff western margin of SW domain.

C) Overview of the sandstone–conglomerate sequence of the Atshan Formation at Wadi Atshan. The lower part consists of bedded fluvial–lacustrine sandstone, which is folded and offset by normal faults. The rectangles labeled 'D' and 'E' indicate the locations of Fig. 7D and E, respectively. Looking south.

D) Close-up view of fluvial sandstone of the Atshan Formation at Wadi Atshan, with pebbly layers and mud drapes in the lower part of the cliff shown in Fig. 7C. Looking south from Wadi Atshan.

E) Close-up view of muddy matrix-supported conglomerate above fluvial sandstone, Wadi Atshan. The clasts are poorly sorted and angular. The photograph shows a large block that fell from the cliff (Fig. 7C). Looking south from Wadi Atshan.

F) Close-up view of well-bedded mudstone and poorly sorted sandstone of the Atshan Formation, NE domain, containing fluvial–lacustrine sediments with mud drape layers. Looking south from small wadi at NE domain.

G) Close-up view of muddy matrix-supported breccia of the Atshan Formation, Wadi El-Dabbah, eastern NE domain. This is a >20-m-thick debris flow deposit that formed in a channel within the bedded mud and sandstone sequence. Looking south at Wadi El-Dabbah.

H) Well-bedded red bed sequence within the Hammamat Group. The alternating red sandstones and shales contain ripple marks, desiccation cracks, and rain drop structures. Main stream of Wadi Atshan, western NE domain. Looking east along west branch of Wadi Atshan.

Fig. 8.

A-1) Tera–Wasserburg concordia plot of zircon age data from the Hammamat Group sample (150323-06). Three Archean grains (~2660 Ma) and one Orosirian grain (~1870 Ma) were analyzed.

A-2) Histogram and relative probability distribution of zircon ages from sample 150323-06 (146 analyses, 145 grains). Most of the grains record ages of 1100–640 Ma, with peaks at 790, 680, and 650 Ma.

B-1) Tera–Wasserburg concordia plot of zircon age data from the quartz porphyry (sample 160320-53). B-2) Histogram and relative probability distribution of zircon ages from sample 160320-53 (49 analyses, 49 grains). There are two age peaks at ~650 and 680 Ma.

C-1) Tera–Wasserburg concordia plot of zircon age data from the quartz porphyry (sample 160321-52).

C-2) Histogram of single-zircon age data, sample 160321-52 (50 analyses, 50 grains). The mean age is 659.6 ± 3.0 Ma.

D-1) Tera–Wasserburg concordia plot of zircon age data from the hornblende–biotite granite (sample 160318-45).

D-2) Histogram of single-zircon age data, sample 160318-45 (48 analyses, 48 grains). The weighted-mean age is 638.1 ± 2.9 Ma.

Fig. 9. Chronostratigraphy of the Wadi El-Dabbah area. Detrital zircon ages, in Ma, of the Hammamat Group are shown by the colored ovals. The Geological stratum show the stratigraphic and intrusion ages. Labels A–D indicate the units from which new zircon ages were obtained. The Geological events and Stages in the El-Dabbah area shown in middle portion. Three main geological stages were identified and each stage was associated with sedimentation ($Sed_{1–3}$), Intrusion (Int.) and deformation ($D_{1–3}$) . The right column shows the regional deformation events recognized within the Arabian–Nubian Shield (Stern and Johnson, 2010; Fritz et al., 2013).

Fig. 10. Model of D_2 extension. The NNE side down normal fault (F_2) and the north-south oriented sinistral strike-slip Wadi Dabbah fault (F_3) were active after intrusion of the granite and the quartz porphyry.

Fig. 1

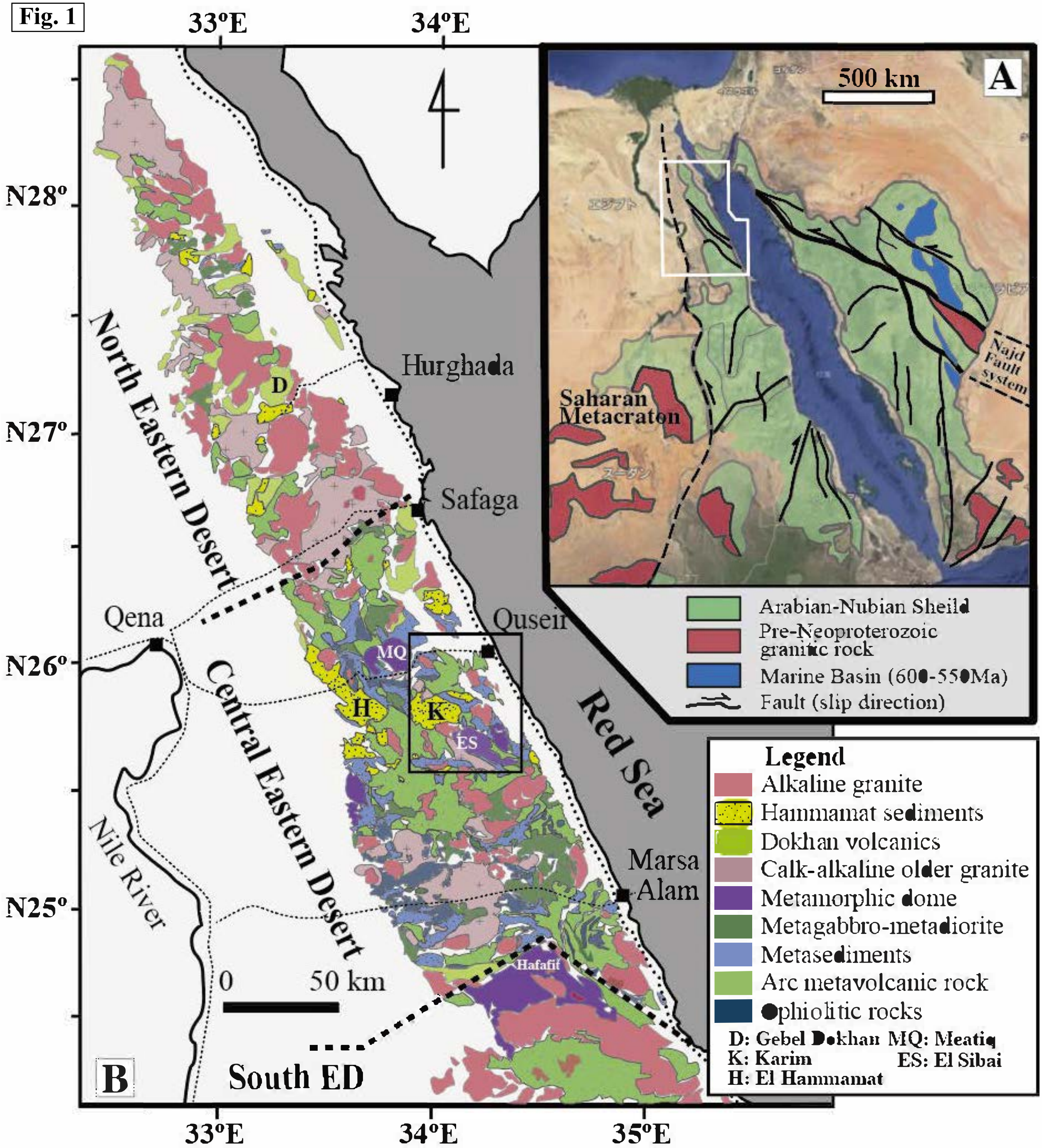
33°E
34°E
35°E
N28°
N27°
N26°
N25°
North Eastern Desert
Central Eastern Desert
South ED
Nile River
Hurghada
Safaga
Qena
Qusier
Marsa Alam
Hafafit
Red Sea
D
MQ
H
K
ES
0
50 km
B
500 km
A
Saharan Metacraton
Najd Fault system
エジプト
スーダン
Arabian-Nubian Sheild
Pre-Neoproterozoic granitic rock
Marine Basin (600-550Ma)
Fault (slip direction)
Legend
Alkaline granite
Hammamat sediments
Dokhan volcanics
Calk-alkaline older granite
Metamorphic dome
Metagabbro-metadiorite
Metasediments
Arc metavolcanic rock
Ophiolitic rocks
D: Gebel Dokhan
MQ: Meatiq
K: Karim
ES: El Sibai
H: El Hammamat

Fig. 2

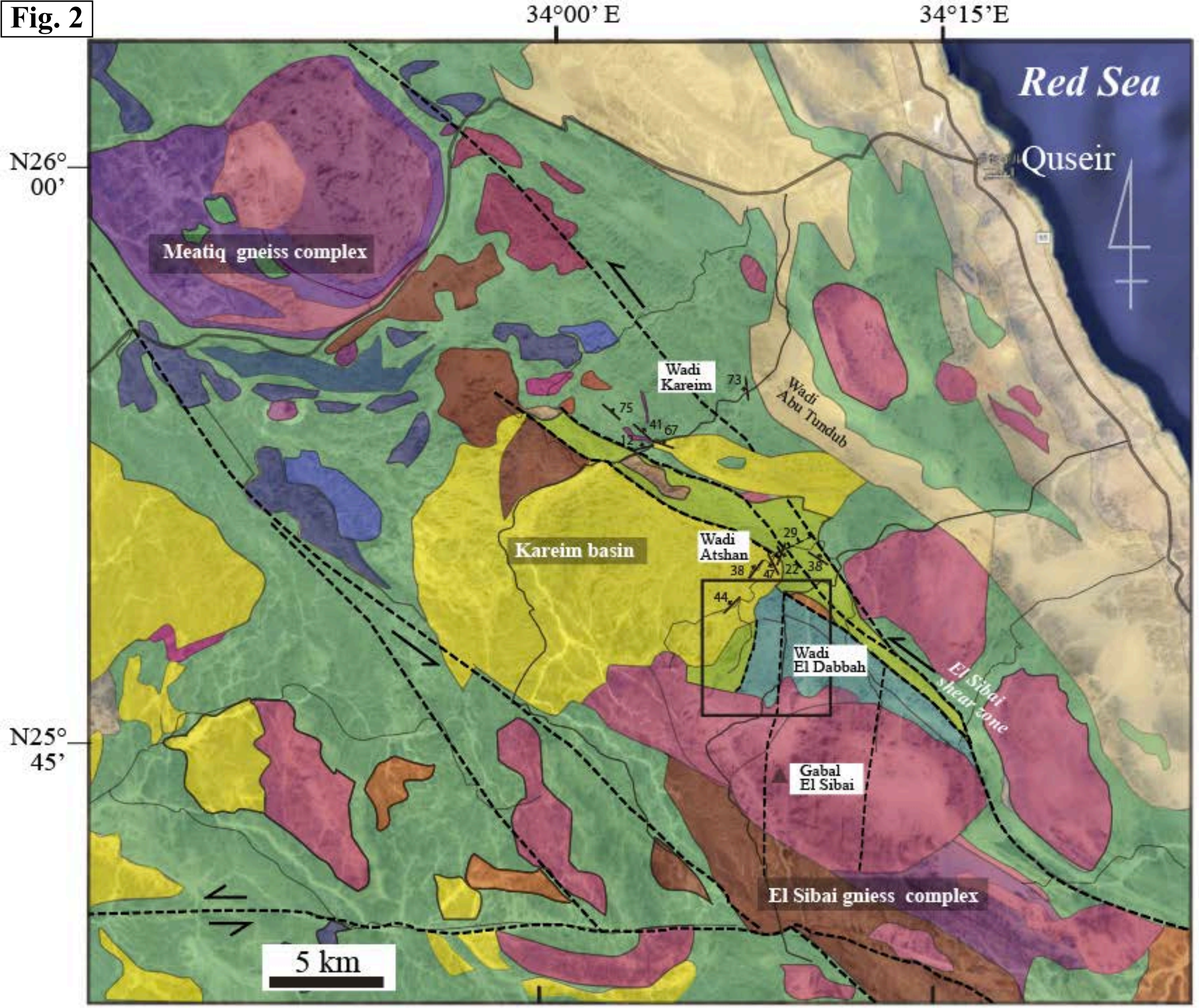

Regend

- Phanerozoic sediments
- Leucogabbro (540 Ma)
- Hammamat Group (600-550 Ma)
- Metasediment sequence (Atshan Formation) (680-660 Ma)
- Volcaniclastics sequence with iron formations (El Dabbah Group) (750-680 Ma)
- Volcaniclastics sequence (unclassificated) (550 Ma)
- Post tectonics granitic rock (660-640 Ma)
- Calc-alkaline older granitic rock
- Metamorphic gneiss complex
- Serpentinites
- Ophiolitic gabbros

Fault (strike-slip)

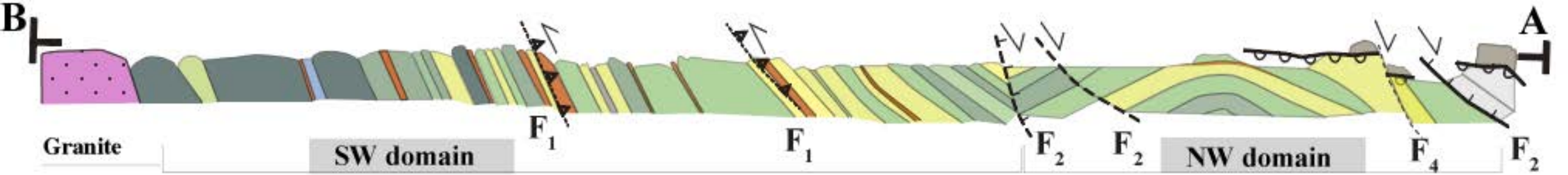
B
A
F1
F1
F2
F2
F4
F2
Granite
SW domain
NW domain

Fig. 3

E 34° 7'

E 34° 10'

N 25°50'

N 25°49'

N 25°48'

N 25°47'

A

B

Wadi Atsham

Wadi El-Dabbah

15-0323-06

16-0320-53

16-0320-52

16-0318-45

F_1

F_2

F_2 (F_3)

F_4

NW domain

NE domain

SW domain

SE domain

El-Dabbah Fault

RW 00 RW 01 RW 02 RW 03 RW 04 RW 05 RW 06 RW 07 RW 08 RW 09 RW 10 RW 11 RW 12 RW 13 RW 14

RE 01 RE 02 RE 03 RE 04 RE 05 RE 06 RE 07 RE 08 RE 09 RE 10 RE 11 RE 12 RE 13 RE 14 RE 15

mine

0 1 km

Legend

Hammamat Group
Qz rich red-purple sandstone/shale

Atshan Formation
muddy matrix conglomerate sandstone/shale

El-Dabbah Group
banded iron formation rich fine volcaniclastics
greeish shale
black shale
bedded, laminated volcaniclastics
pillow lava
massive volcanics
foliated coarse basalt
massive coarse metavolcanics
quartz porphyry
granite

unconformity
thrust fault (F_1)
normal fault (F_2)
El Dabbah fault (F_3) strike-slip fault
normal fault (F_4)
folding (antform)
RW 10 RE 11 wadi branch
age dating point

A

B

F_2

F_4

F_2

F_2

F_1

F_1

NW domain

SW domain

Granite

Fig. 4

A)

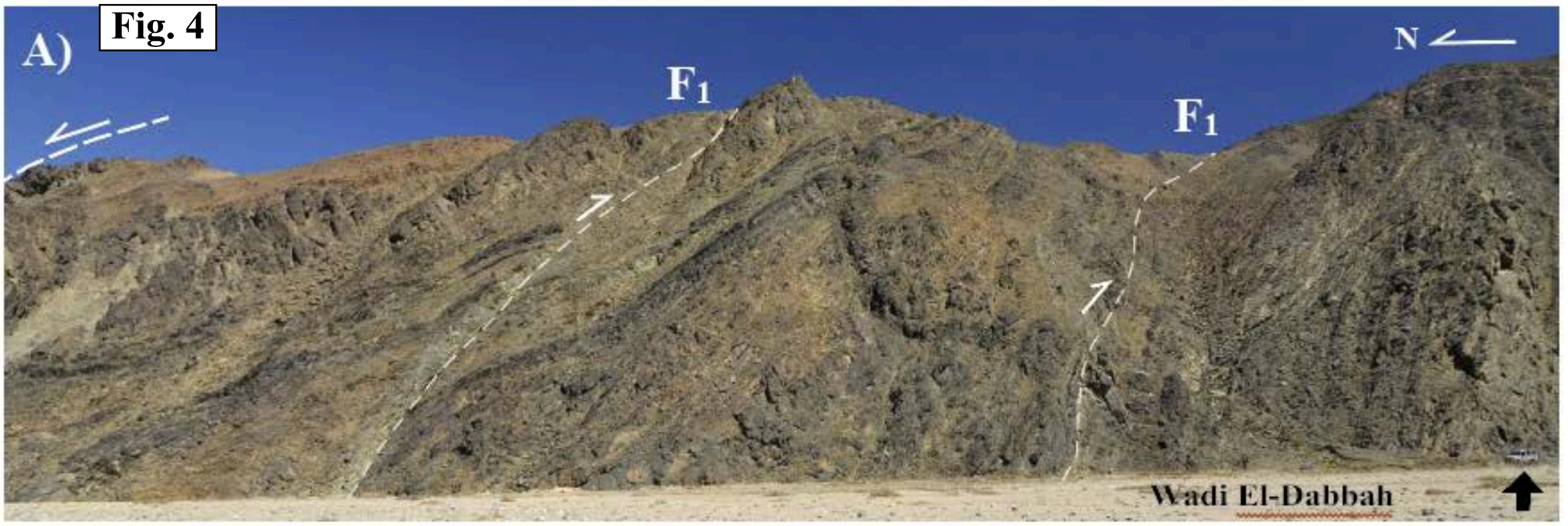
N
F1
F1
Wadi El-Dabbah


B)
RW 8

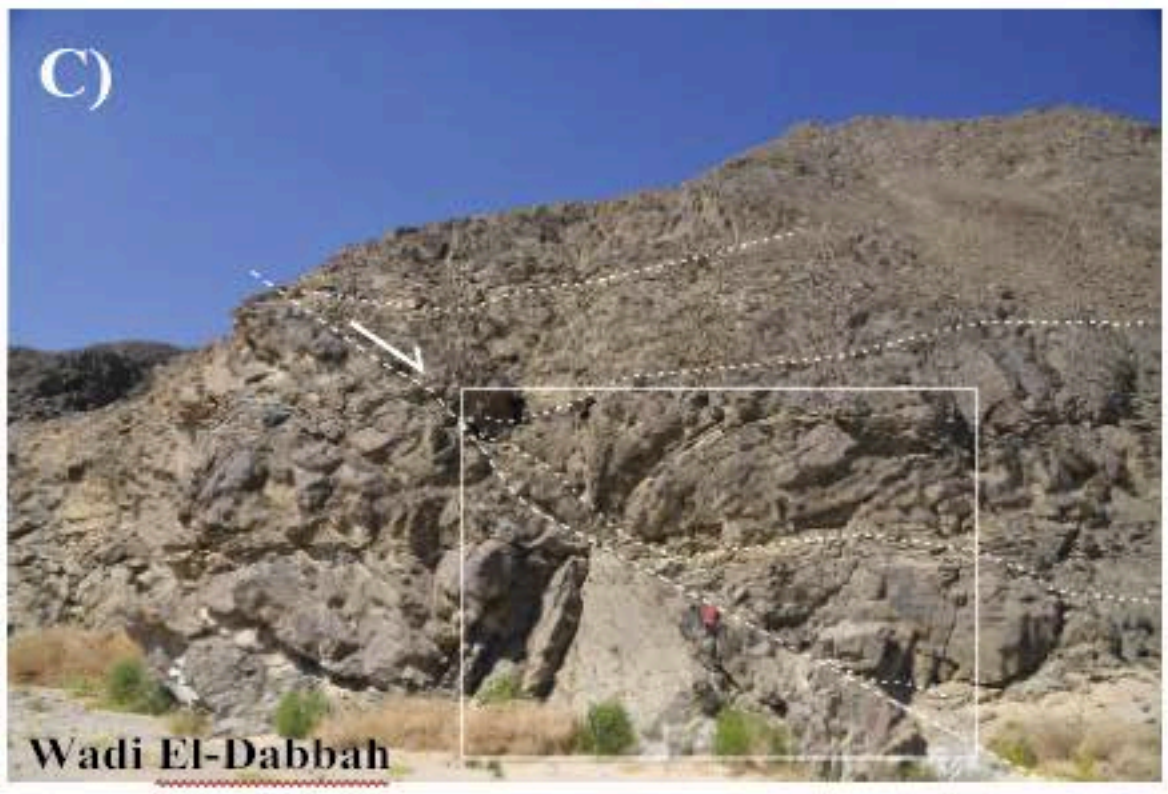
C)
Wadi El-Dabbah

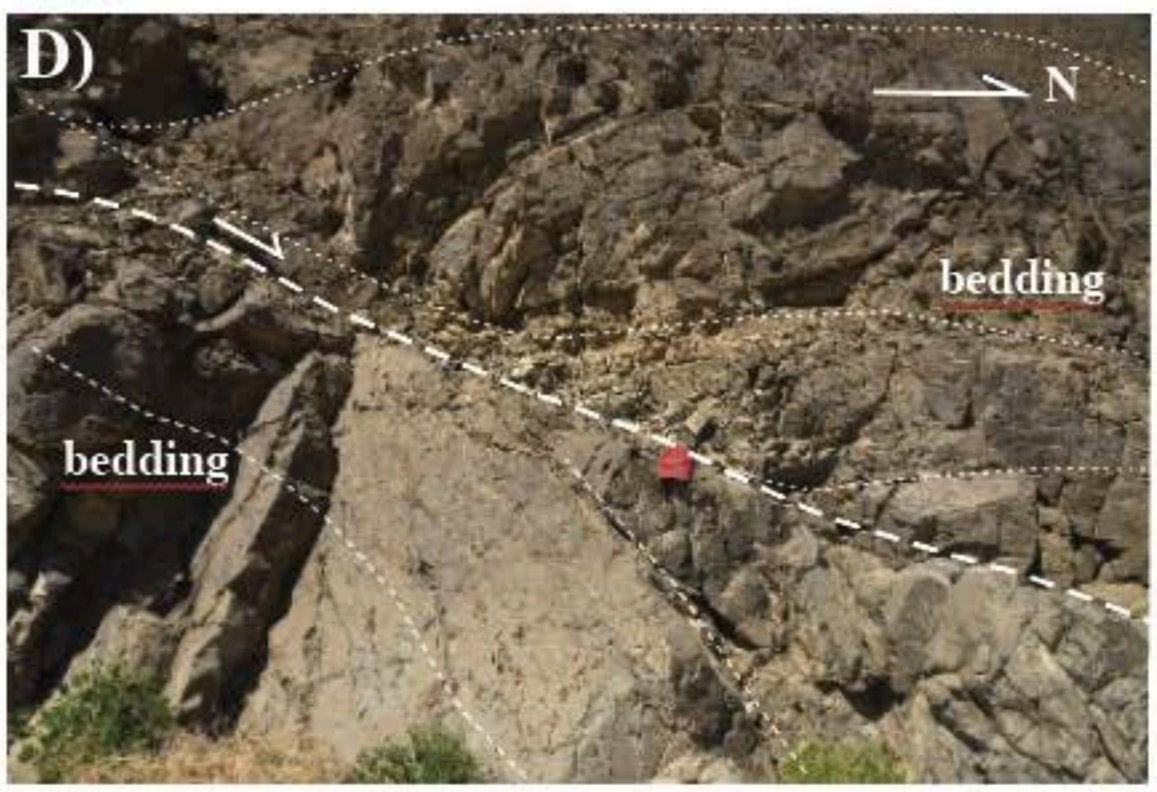
D)
N
bedding
bedding

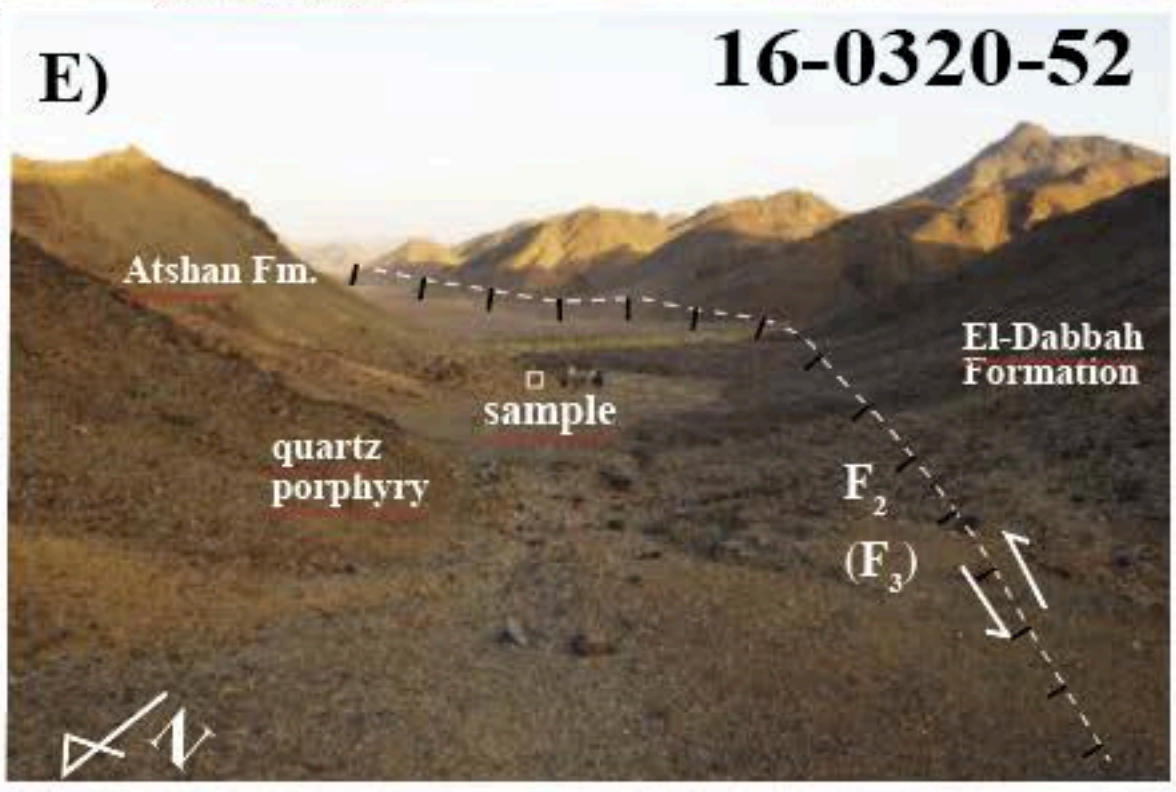
E)
16-0320-52
Atshan Fm.
El-Dabbah Formation
sample
quartz porphyry
F2
(F3)
N

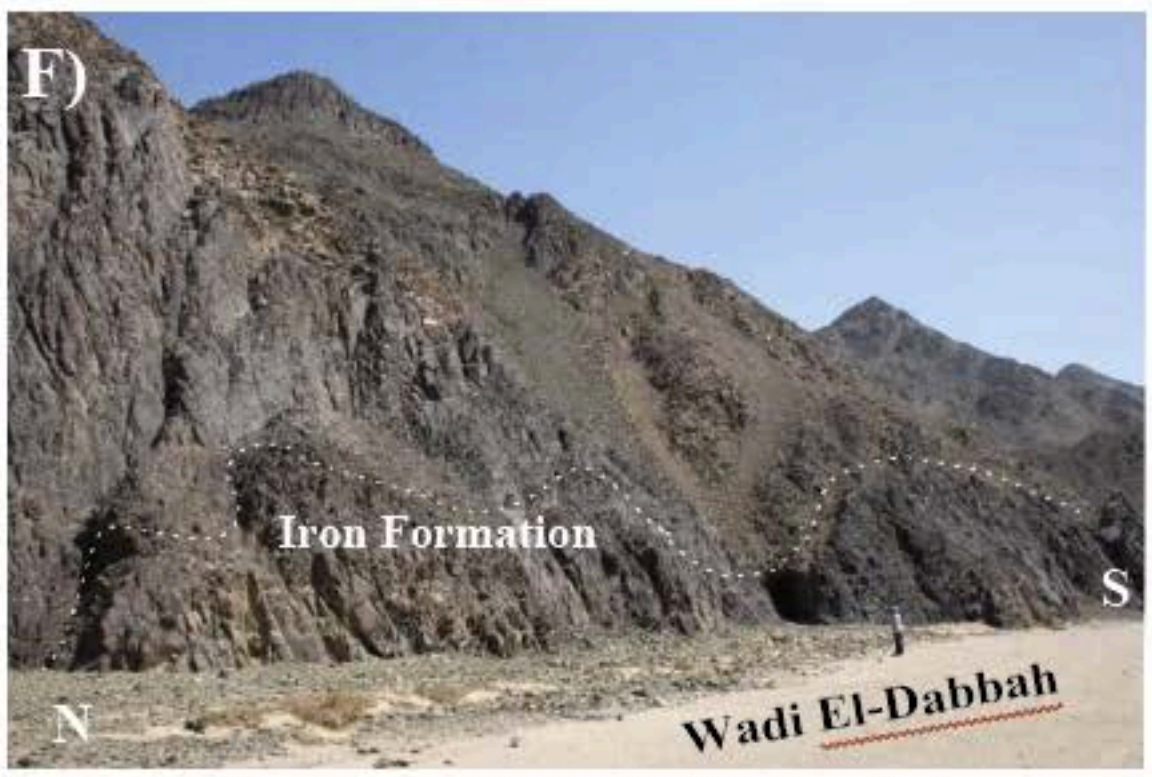
F)
Iron Formation
S
N
Wadi El-Dabbah


G)
16-0318-45
1m

Fig. 5

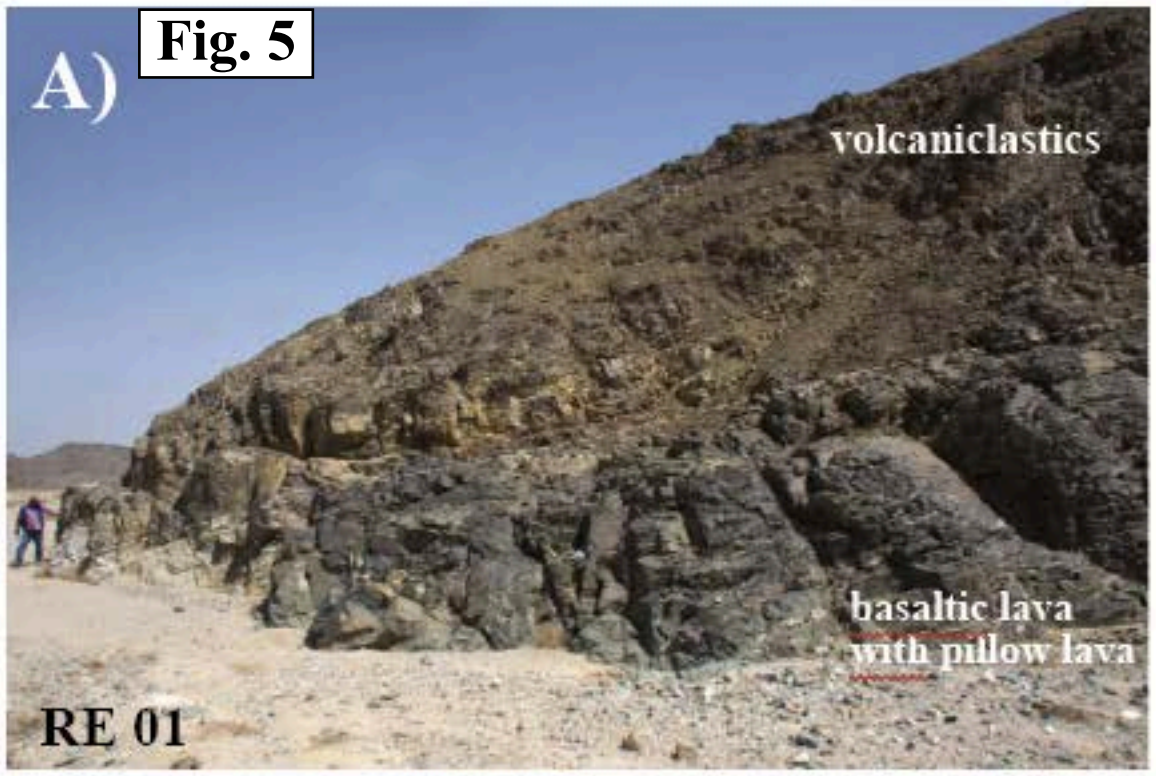
A)
volcaniclastics
basaltic lava
with pillow lava
RE 01


B)
RE 11


C)
RE 5

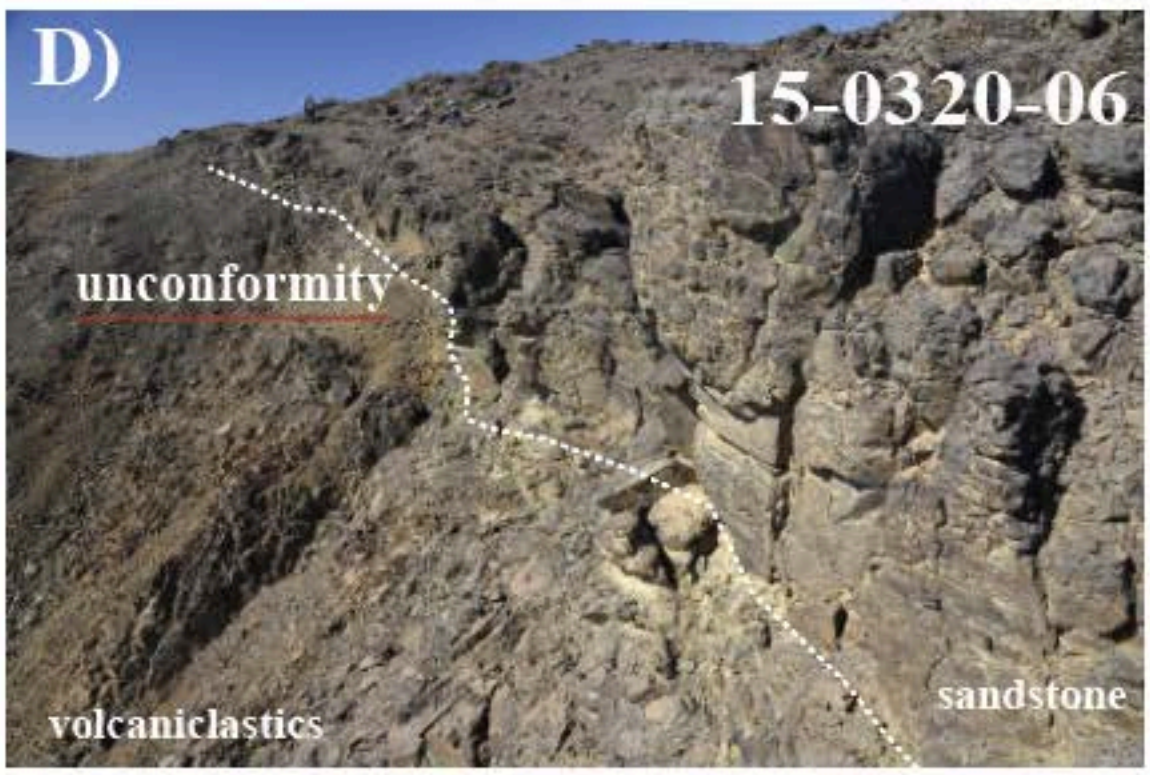
D)
15-0320-06
unconformity
volcaniclastics
sandstone


E)
RW 7


F)
RW 7


G)
RW 7


H)
RW 6

Fig. 6

Geologic columns at Wadi El-Dabbah area

(km)

9
8
7
6
5
4
3
2
1
0

Hammamat Group

Atshan Fm.

El-Dabbah Group

Hammamat
sandstone/green, red shale /conglomerate (fluvial, flood plain)

Unconformity

Atshan
sandstone/mudstone (fluvial, lacustrine sediments)

Unconformity

(Domain name)

Upper ED Fm.
fine volcaniclastics sediments
accretionary lapilli
basaltic pillow lava

Middle ED Formation
fine-medium volcaniclastics sediments
pillow lava volcanclastics
iron formation
(iron mine)
basaltic pillow lava volcaniclastics

Lower ED Formation
massive coarse volcanics thin layers of volcaniclastic rocks
massive coarse volcanics
microgabbro

NW domain
NE
SW domain
SE domain

Column of the El-Dabbah Group at SW domain

(km)

4
3
2
1
0

Wadi branch name

RW 03
basaltic pillow lava

RW 04
accretionary lapilli
massive volcanics

RW 05
volcaniclastics iron formation
basaltic pillow lava

volcaniclastics iron formation

RW 07
basaltic pillow lava
volcaniclastics iron formation

RW 08
accretionary lapilli
basaltic pillow lava

RW 10
volcaniclastics

RW 11
volcaniclastics iron formation (IF/jasper) pale greenish shale

RW 12
accretionary lapilli volcaniclastics
massive volcanics
basaltic pillow lava

RW 13
massive coarse volcanics
thin layers of volcaniclastic rocks IF/jasper beds

Upper ED Formation

Middle ED Formation
Volcaniclastics Member
BIF Member

Lower ED Fm.

Legend

- fine laminated volcaniclastics
- iron formation (BIF, jasper)
- well laminated pale greenish shale
- laminated greenish-black shale
- bedded volcaniclastics
- massive volcanics basaltic pillow lava
- massive coarse volcanics (microgabbro)
- sandstone detrital zircon age

Fig. 7

A)

B)

C)

D)

E)

F)

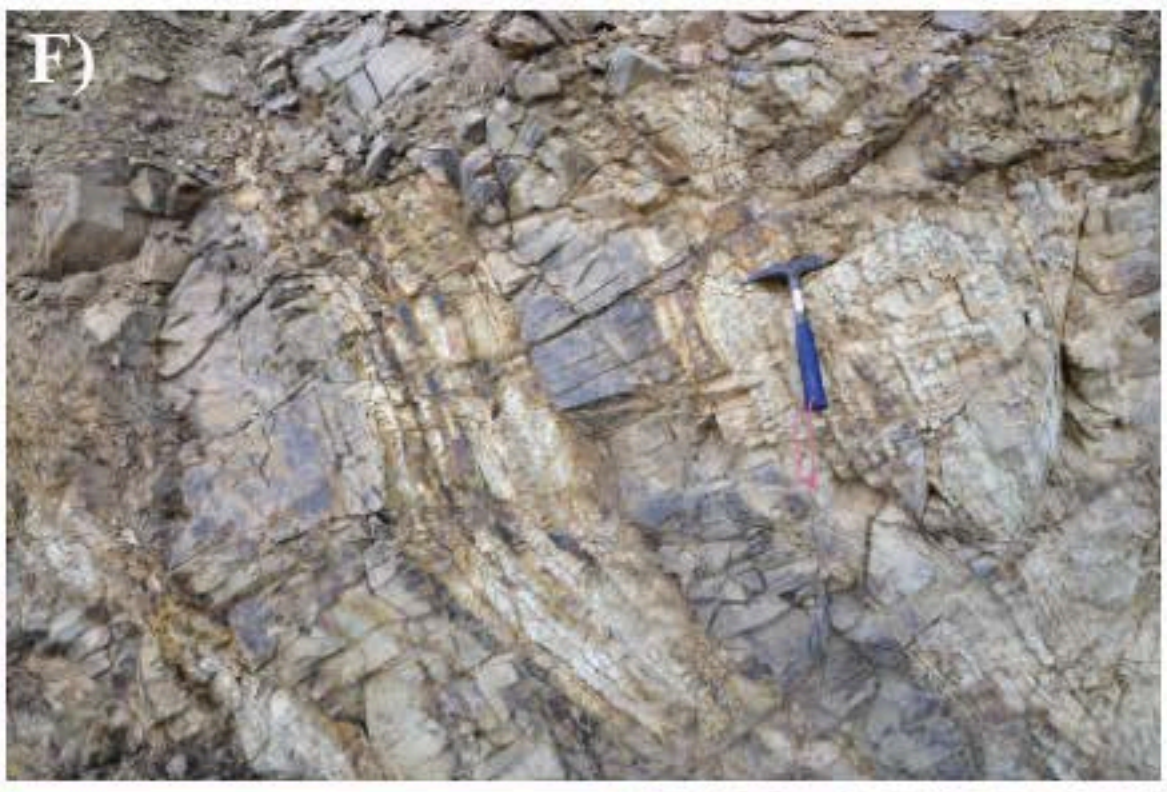

G)

H)

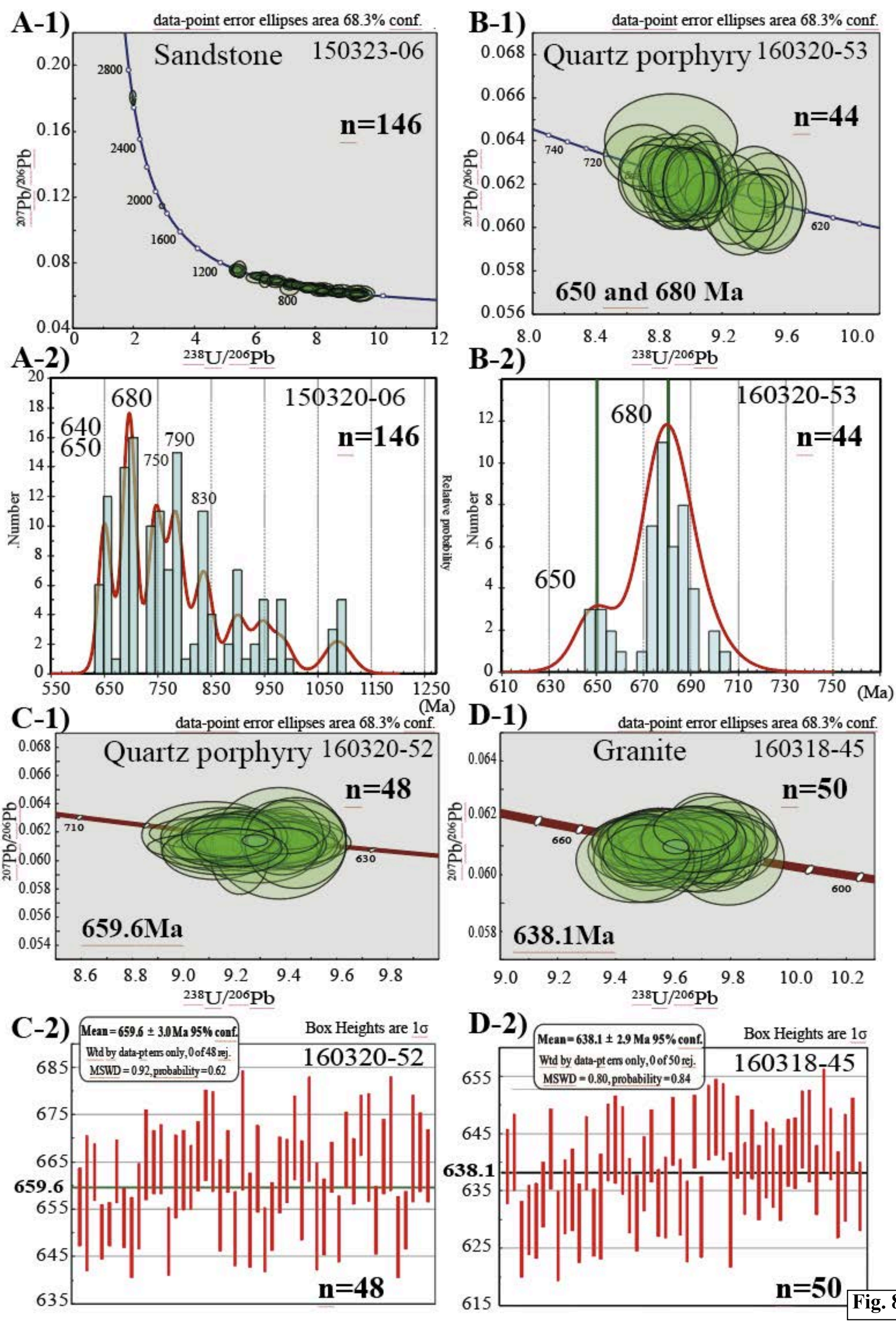
A-1)
data-point error ellipses area 68.3% conf.
Sandstone 150323-06
n=146
2800
2400
2000
1600
1200
800
0.20
0.16
0.12
0.08
0.04
0
2
4
6
8
10
12
207Pb/206Pb
238U/206Pb
B-1)
data-point error ellipses area 68.3% conf.
Quartz porphyry 160320-53
n=44
740
720
620
650 and 680 Ma
0.068
0.066
0.064
0.062
0.060
0.058
0.056
8.0
8.4
8.8
9.2
9.6
10.0
207Pb/206Pb
238U/206Pb
A-2)
680
640
650
790
750
830
150320-06
n=146
Number
Relative probability
550
650
750
850
950
1050
1150
1250
(Ma)
B-2)
680
650
160320-53
n=44
Number
610
630
650
670
690
710
730
750
(Ma)
C-1)
data-point error ellipses area 68.3% conf.
Quartz porphyry 160320-52
n=48
710
630
659.6Ma
0.068
0.066
0.064
0.062
0.060
0.058
0.056
0.054
8.6
8.8
9.0
9.2
9.4
9.6
9.8
207Pb/206Pb
238U/206Pb
D-1)
data-point error ellipses area 68.3% conf.
Granite 160318-45
n=50
660
600
638.1Ma
0.064
0.062
0.060
0.058
9.0
9.2
9.4
9.6
9.8
10.0
10.2
207Pb/206Pb
238U/206Pb
C-2)
Mean = 659.6 ± 3.0 Ma 95% conf.
Wtd by data-pt errs only, 0 of 48 rej.
MSWD = 0.92, probability = 0.62
Box Heights are 1σ
160320-52
659.6
n=48
685
675
665
655
645
635
D-2)
Mean = 638.1 ± 2.9 Ma 95% conf.
Wtd by data-pt errs only, 0 of 50 rej.
MSWD = 0.80, probability = 0.84
Box Heights are 1σ
160318-45
638.1
n=50
655
645
635
625
615

Fig. 8

Time scale

(Ma)

600

635
Marinoan glaciation
640

660

700

Sturtian glaciation
717

800

Ediacaran

Cryogenian

Zircon age (Ma)

583
Wilde and Youssef (2002)

sandstone zircon age

640-650

680

693
Abd El-Rahman et al. (2019)

Khalil et al. (2015)
718
725
El-Shazly and Khalil (2016)

750

766
El-Shazly and Khalil (2016)

790

830

Geological stratum

Hammamat Group
A

D 638
B C 660

Atshan Formation

El-Dabbah Group

?

Geological events in El-Dabbah area

normal fault (F_4)

El Dabbah fault
strike-slip (F_3)
normal fault (F_2)

Intrusion granite
quartz porphyry

Island arc accretion
thrust (F_1)

Island arc volcanic activity

Transtension
El-Sibai shear zone

Geological Stages

Stage 3
D_3
Sed 3

Stage 2
D_2
Int.
Sed 2

Stage 1
D_1
Sed 1

Regional tectonic phase

north — south

Najd fault system
Metamorphic dome

Orogenic collapse

East African Orogeny

Arabian-Nubian shield island arc formation accretion stage

Juvenile crust production phase

Rifting of Rodinia

Wilde and Youssef (2000)
Breitkreuz (2010)
Dokhan volcanism
(570 -530 Ma)
Alkali granite (post collision)
(630 -570 Ma)
Calc-alkali granite
Meatiq dome
Kareim basin
El-Sibai
NW stretching
(630 -590 Ma)
Fowler et al. (2007)
Augland et al. (2012)

Bregar et al. (2002)
Augland et al. (2012)
(670 -690 Ma)
Top to North (low angle mylonite)
El-Sibai emplacement age

Collision stage

Volcaniclastics /iron formation depositional age
(693~718 Ma)
Khalil et al. (2015)
Abd El-Rahaman et al. (2019)

Arc magmatism

(770 -730 Ma)

Legend

This stady age data
granite
quartz porphyry
detrital sandstone

Previous age data
detrital sandstone
metavolcanics at Central Eastern Desert

Fig. 9

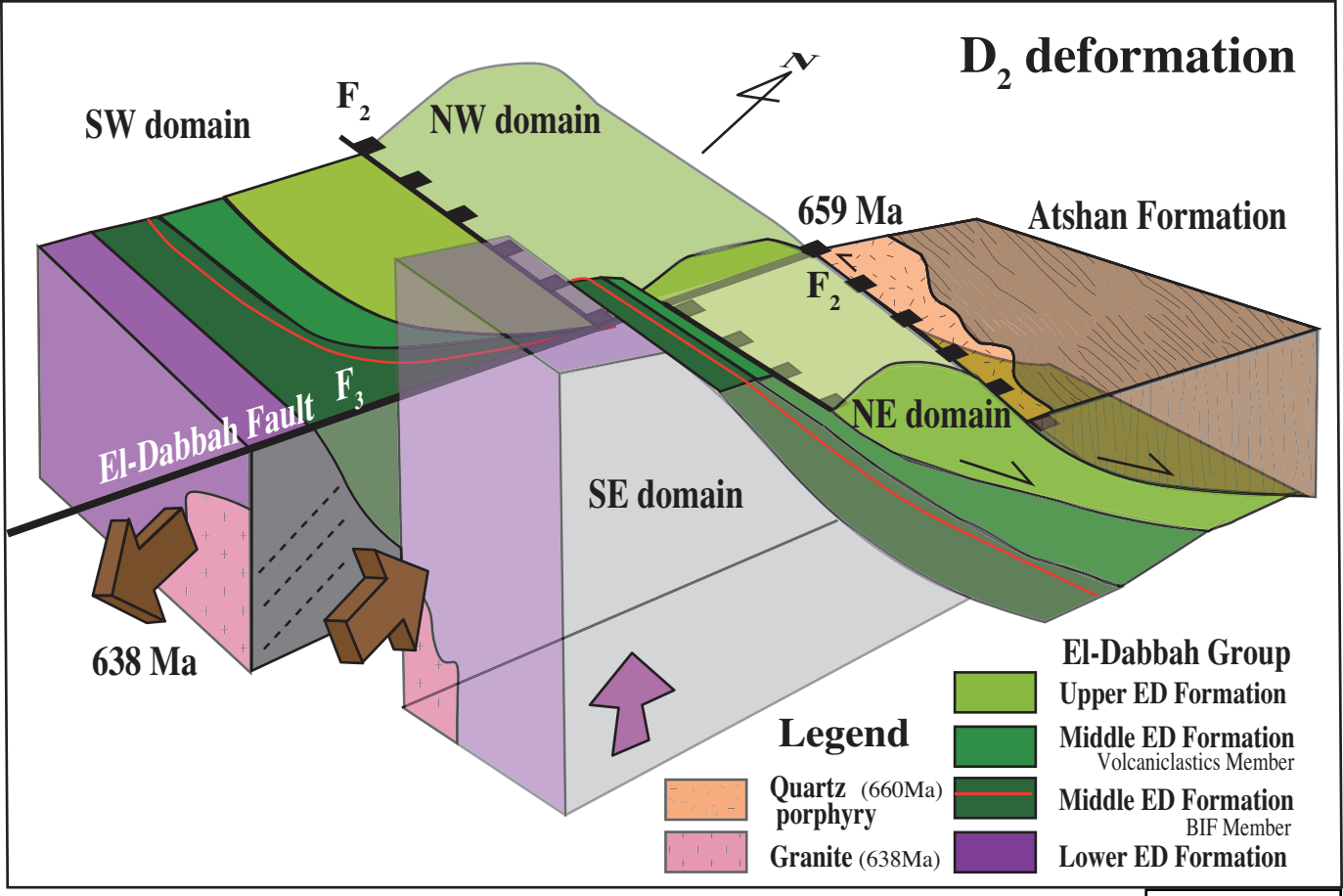
D2 deformation
SW domain
F2
NW domain
N
659 Ma
Atshan Formation
F2
NE domain
El-Dabbah Fault
F3
SE domain
638 Ma
El-Dabbah Group
Upper ED Formation
Middle ED Formation
Volcaniclastics Member
Middle ED Formation
BIF Member
Lower ED Formation
Legend
Quartz (660Ma) porphyry
Granite (638Ma)

Fig. 10

(F2)